CHAPTER 4

Experimental investigation

This chapter presents a comparative study on performance of a CO_2 trans-critical refrigeration system equipped with internal heat exchanger (IHX), operating in warm climate (up to 45ºC), based on experimental data in energetic and exergetic perspective. Experiments are conducted for two sets of evaporator temperatures (-5ºC and 0ºC) and for four different ambient temperatures (32ºC, 35ºC, 40ºC and 45ºC) for a range of gas cooler pressure within 80 to 110 bar. The investigated parameters include refrigeration capacity, compressor power, effectiveness of IHX, compressor discharge temperature, approach temperature, exergetic efficiency and irreversibility contribution of the cycle components. The study in this chapter investigates a prominent research gap of effect of gas cooler face velocity on energetic and exergetic parameters apart from the novelty of the indigenous CO_2 refrigeration experimental setup.

4.1 Experimental setup

An experimental refrigeration setup is designed and fabricated for CO_2 trans-critical vapor compression cycle to experimentally investigate at high ambient (near 45ºC). The same is installed at the Thermal Science Laboratory under The Department of Mechanical Engineering at Birla Institute of Technology and Science, Pilani, Campus, shown in Fig. 4.1. The local atmosphere is arid and over the year the ambient outdoor temperature varies form -2ºC in winter (December-January) to 48ºC in summer (June-July). The indoor temperature in the laboratory however remains within 0ºC to 45ºC. There is also considerable variation of temperature across the day on most days. The schematic for CO_2 trans-critical refrigeration test rig equipped with IHX is shown in Fig. 4.2.

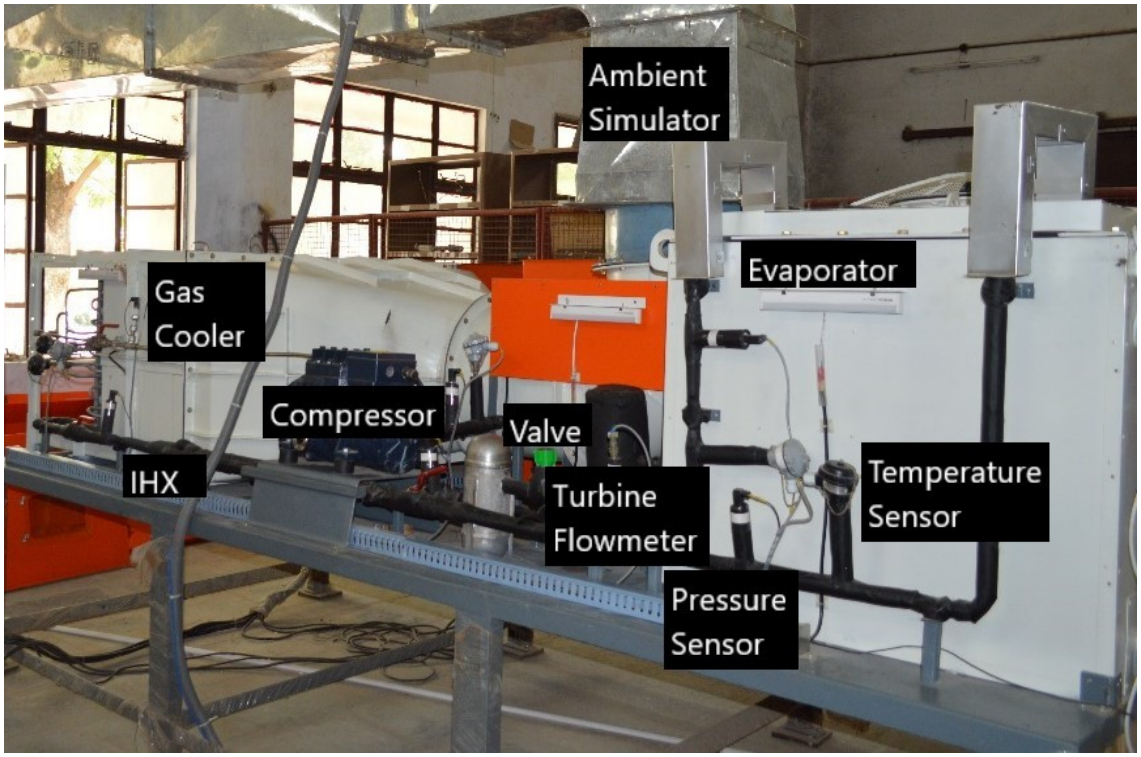

Fig. 4.1 Photograph of the CO_2 trans-critical refrigeration system equipped with IHX

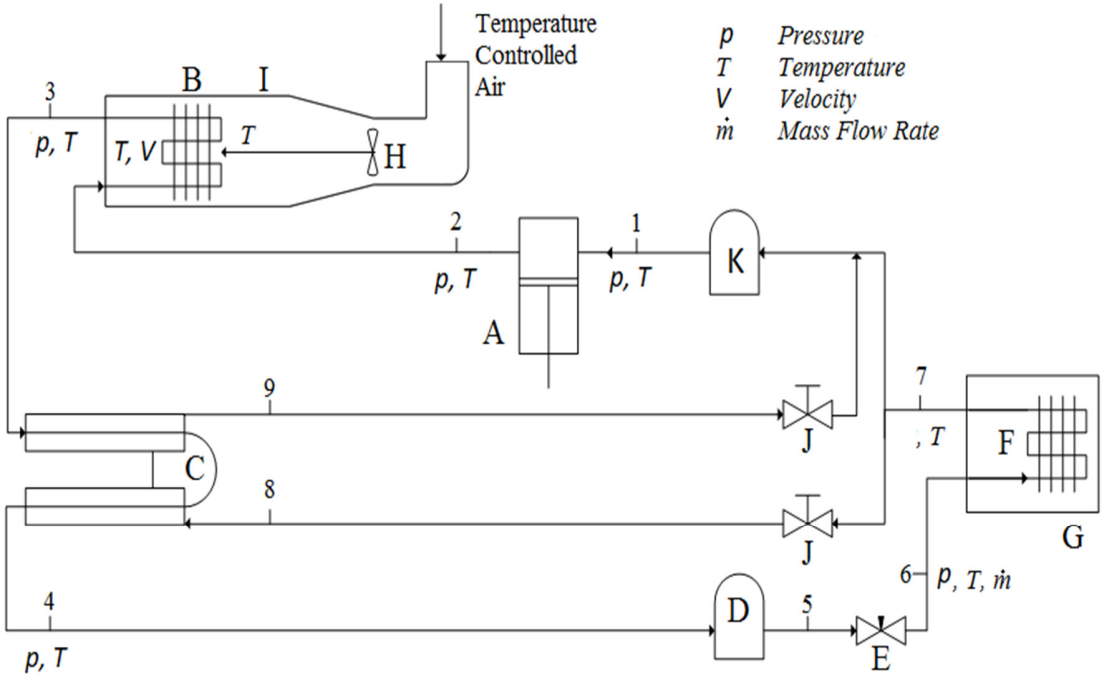

Fig. 4.2 Schematic of the CO_2 trans-critical refrigeration system equipped with IHX

4.1.1 Compressor

A semi hermetic compressor (Dorin; Model CD 360H) is used in the experimental setup with expected compression ratio of 2 to 4. The features (along with photograph) and specifications of CO_2 compressor are given in Fig. 4.3 and Table 4.1, respectively. The operating conditions are limited to minimum of 10 bar of suction pressure, maximum of 120 bar for outlet pressure and a maximum of 180ºC for discharge temperature.

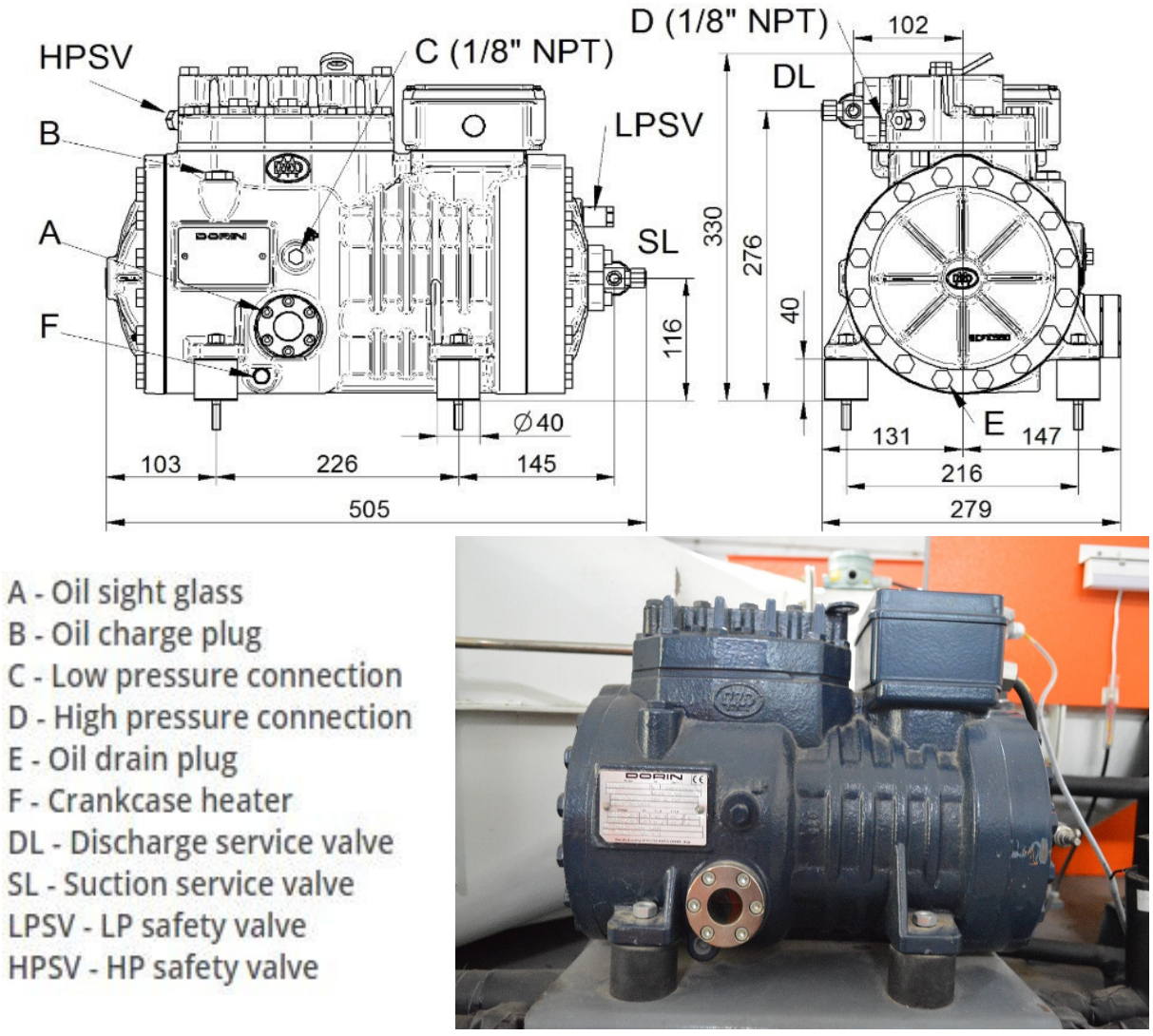

Fig. 4.3 Features and photograph of compressor (Dorin CD 360H)

Table 4.1 Specification of compressor

Model	Dorin CD 360H
Input phase/voltage/frequency	3-phase/380-420 V/50 Hz
No of cylinders	2
Net weight	78 kg
Capacity	5 kW
Bore/stroke	25 mm/ 28 mm
Displacement	2.39 m^3/h
RPM @ 50 Hz	1450
Oil	Dorin CL80
Oil charge	1.3 kg
Superheat	10°C
Maximum discharge pressure	120 bar
Minimum suction pressure	10 bar
Maximum discharge temperature	180°C

The compressor comes with some standard safety features which include Thermik protection, Electrical box IP65 and low as well as high pressure relief valves. The input to the compressor is controlled using variable frequency within range 1200-1600 rpm at the maximum current frequency of 50 Hz. The system is charged through the suction service valve as shown in Fig. 4.3. The maximum operating current is 9.4 A while the locked rotor current is 43.5 A.

4.1.2 Gas cooler

A finned tube air cooled type gas cooler is designed and fabricated with the help of local manufacture Hemair, Hyderabad in India. The specifications and a photograph of the CO_2 gas cooler are given in Table 4.2 and Fig. 4.4, respectively. Each segment of gas cooler is instrumented with resistance temperature detector (RTD) to have detailed insight of temperature profile within the circuit.

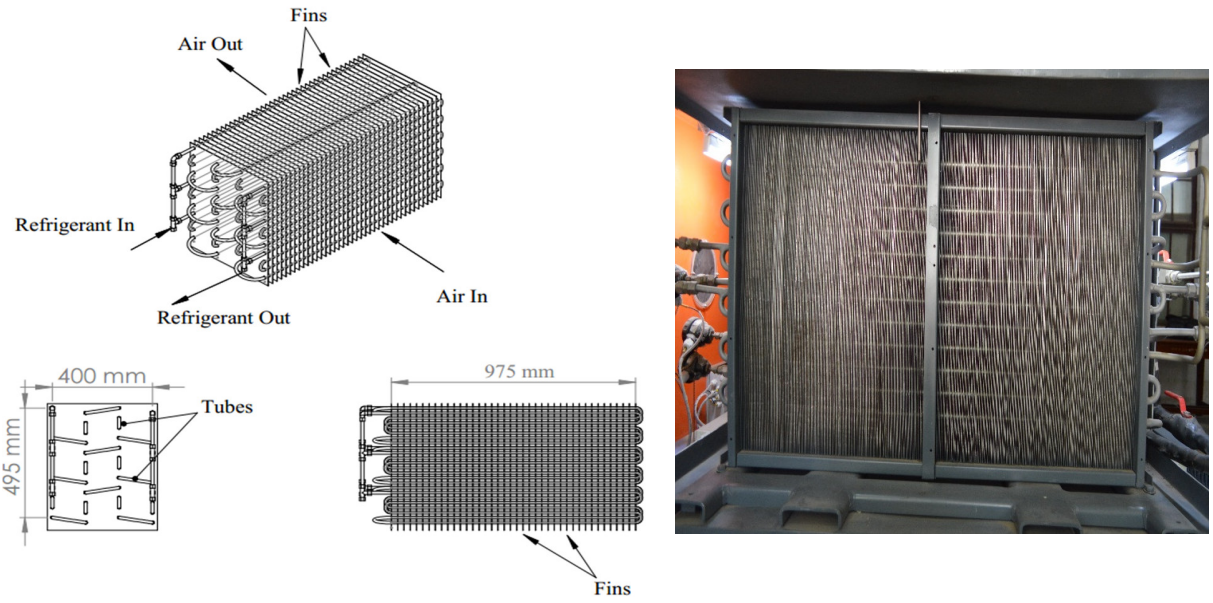

Fig. 4.4 Features and photograph of gas cooler

Table 4.2 Specifications details for gas cooler

Heat exchangers	**Gas cooler**
Material of tube/fins	Copper/Aluminium
Number of pass/circuits	4/3
Number of tubes per pass	4
Inner/Outer diameter of tube (mm)	8.7/12,7
Length of tube (mm)	975
Tube thickness (mm)	2
Tube transverse/longitudinal pitch (mm)	40/70.5
Fin pitch (mm)	1.73
Fin thickness (mm)	0.8

4.1.3 Internal Heat Exchanger (IHX)

A coaxial counter flow IHX is designed and fabricated with the help of local manufacture, Hemair. The features (along with photograph) and specifications of IHX are given in Fig. 4.5 and Table 4.3, respectively. CO_2 at high pressure from the gas cooler is fed into the inner tube of IHX, while the low-pressure CO_2 from the evaporator flows through the outer tube of the IHX. With the help of bypass valve, as shown in Fig. 4.6, the IHX is included or excluded from the loop.

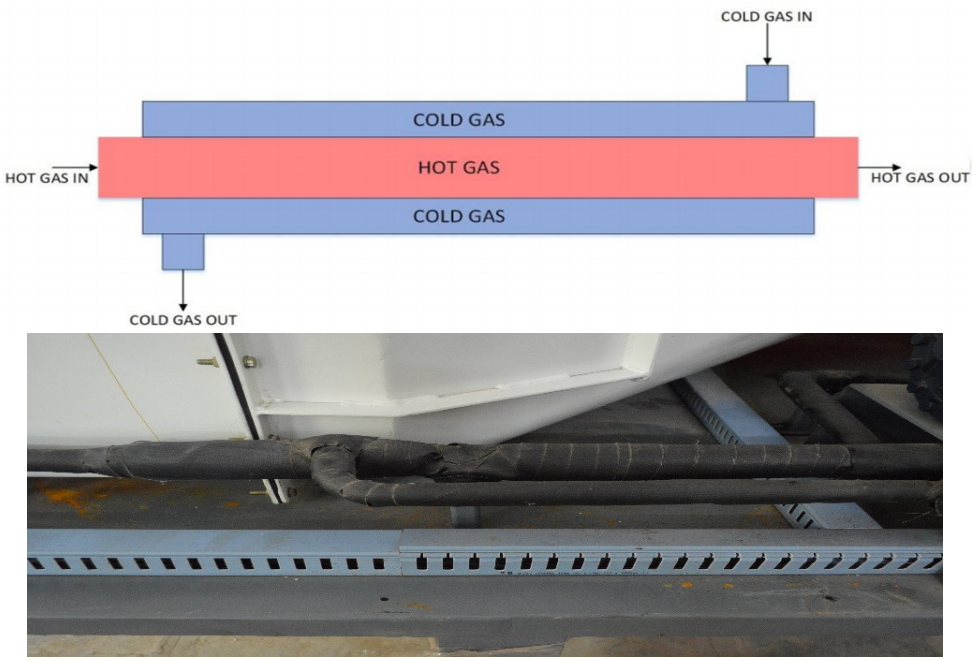

Fig. 4.5 Features and photograph of IHX

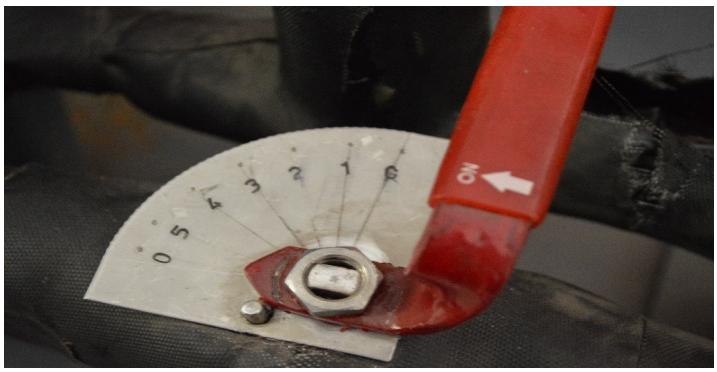

Fig. 4.6 By-pass valve to cater to the IHX

Table 4.3 Specifications details for IHX

Detail	Description
Type	Coaxial, shell and tube type
Material	Stainless Steel
Internal diameter of Inner tube (hot flow) (mm)	19.86
External diameter of Inner tube (hot flow) (mm)	25.40
Internal diameter of outer tube (cold flow) (mm)	45.26
External diameter of outer tube (cold flow) (mm)	50.80
Length of IHX (m)	1.389

4.1.4 Expansion valve

A manual type expansion needle valve of Swagelok make is adopted in experimental setup. The valve is made of stainless steel body with regulating stem and 1/4" inch tube fitting. The maximum inlet pressure is 248 bar with pressure control range of 0.68 bar through 34.4 bar. Flow coefficient (Cv) is 0.39 while the maximum operating temperature is 200°C. The expected minimum and maximum expansion ratios for the valve in experiments are 80/40 and 130/26 bar respectively. Fig. 4.7 depicts the construction details and photograph of the needle valve used in the experiments.

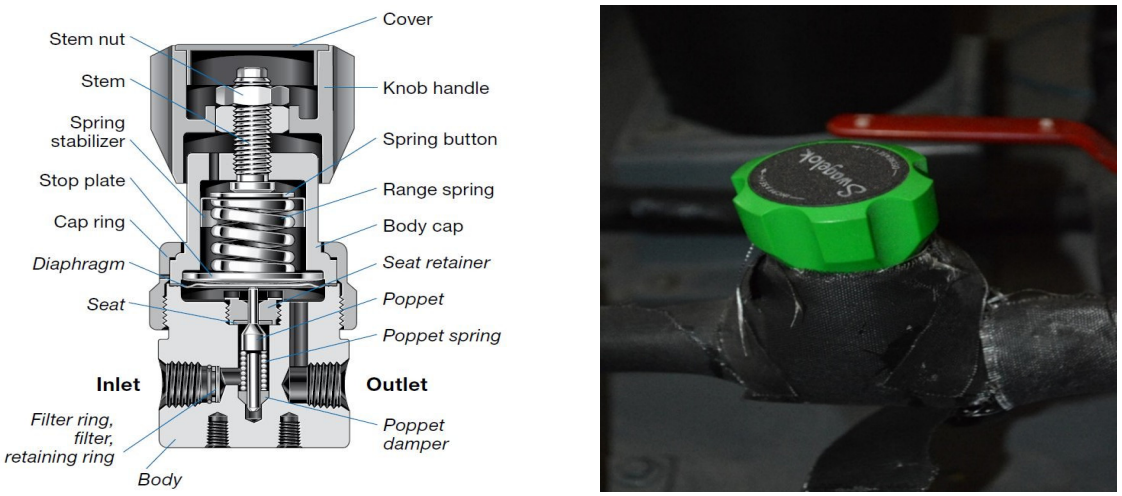

Fig. 4.7 Constructional details and photograph of manual expansion valve

4.1.5 Evaporator

A submerged fin and tube evaporator is designed and fabricated with the help of local manufacture, Hemair. The features (along with photograph) and specifications of CO_2 evaporator are given in Fig. 4.8 and Table 4.4, respectively. An external load simulator in the form of a submerged and metered water heater is applied to maintain the desired cooling capacity. Three submersible pumps of 0.125 HP capacity each are installed in the evaporator tank for churning of the fluid within the tank. The Joule effect of heating due to mechanical work input of submerged

pumps are neglected in the analysis. The desired level of fluid is monitored in the evaporator tank using measuring scale and a balance of flow rate of fluid entering and leaving the evaporator tank is maintained.

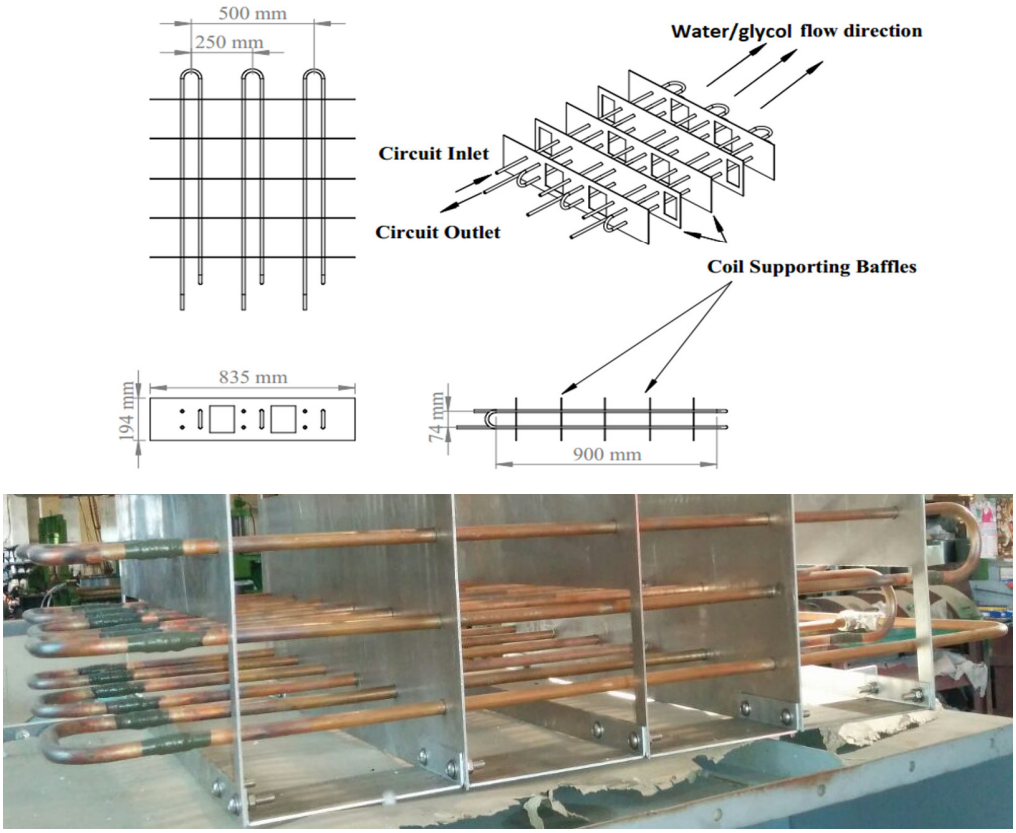

Fig. 4.8 Features and photograph of evaporator

Table 4.4 Specifications details for evaporator

Heat exchangers	**Evaporator**
Material of tube/fins	Copper/Aluminium
Number of pass/circuit	5/3
Number of tubes per pass	2
Inner/Outer diameter of tube (mm)	8.7/12.7
Length of tube (mm)	900
Tube thickness (mm)	2
Tube transverse pitch (mm)	74
Tube longitudinal pitch (mm)	74
Fin pitch (mm)	177
Fin thickness (mm)	3

4.1.6 Accumulator and receiver

The accumulator and liquid receiver are also designed and fabricated with the help of local manufacture, Hemair. The mean height and diameter for both accumulator and receiver are 170 mm and 86 mm, respectively. The body and connectors are made up of stainless steel while the base plate and supporting member are made up of mild steel. Fig. 4.9 and Fig. 4.10 shows construction details for accumulator and receiver, respectively.

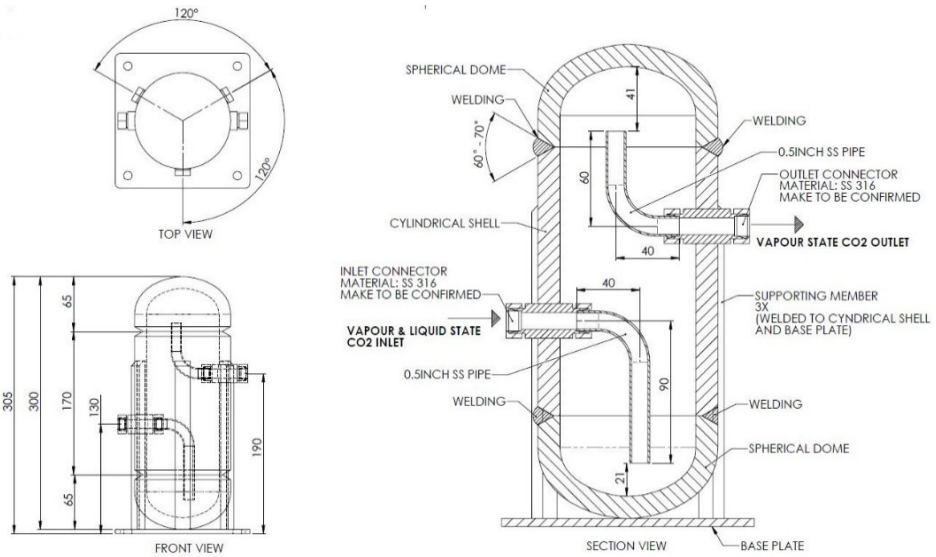

Fig. 4.9 Construction details of accumulator

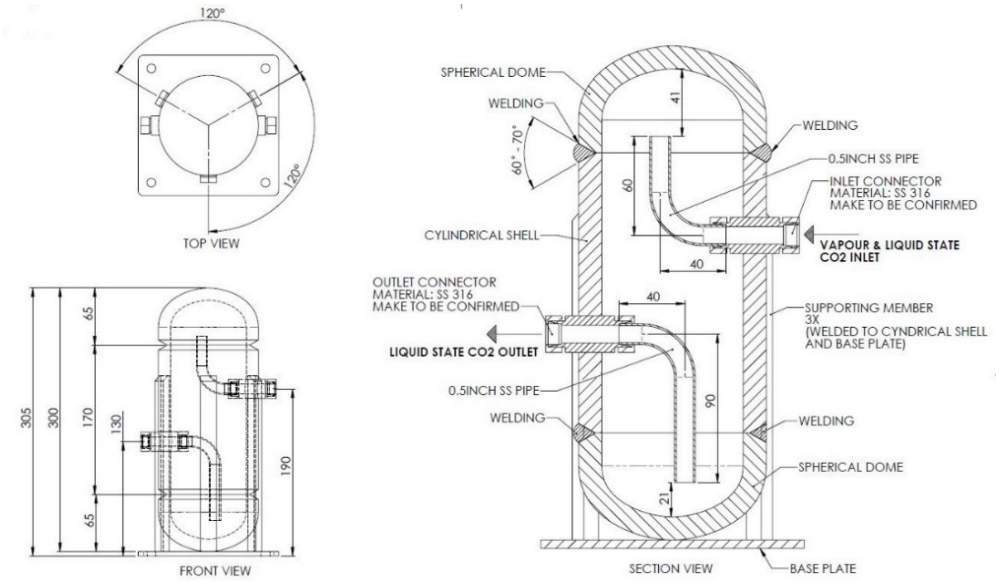

Fig. 4.10 Construction details of receiver

4.1.7 Tubing and fittings

Tubing was designed for maximum pressure of 200 bar. The refrigerant circuit of approximately 15 m in length is made of stainless steel with tube having outer diameter of 12.7 mm (1/2 inch) and inner diameter of 8.7 mm (thickness: 2 mm). Tubes are insulated by asbestos rope covered with foam.

4.1.8 Evaporator load simulator

Evaporator (chiller) load simulator, shown in Fig. 4.11, comprises of a tank accumulating water/ethylene-glycol (50%-50%) along with three heaters for load simulation. Two of the heaters installed are of fixed capacity of 3 kW each and switchable (shown in Fig. 4.12 a), while the third heater of capacity 3 kW is connected via an autotransformer (Fig. 4.12 b) to provide continuously variable load within range 1-9 kW. Two centrifugal pumps of capacity 0.5 HP each are installed to maintain volume flow rate of water/glycol solution in the chiller circuit (Fig. 4.12 c &d). All the tubing for the evaporator load simulator loop are constructed using ceramic pipe with suitable fittings. The flow across the evaporator is controlled using individual valves at inlet and outlet of load simulator.

4.1.9 Ambient load simulator

An ambient temperature simulator is installed, shown in Fig. 4.13, to simulate the required test condition in gas cooler side. It comprises of an air duct with installed inline heaters having maximum capacity 10 kW to heat the incoming air to the required ambient setting before flow over the gas cooler. A tuneable automatic controller, as shown in Fig. 4.14 (a), is installed for maintaining air at intended temperature within ±0.5ºC of set point. A VFD controlled axial fan, as shown in Fig. 4.14 (b) is also installed to simulate the air velocity over the gas cooler within the range of 1 m/s to 3 m/s.

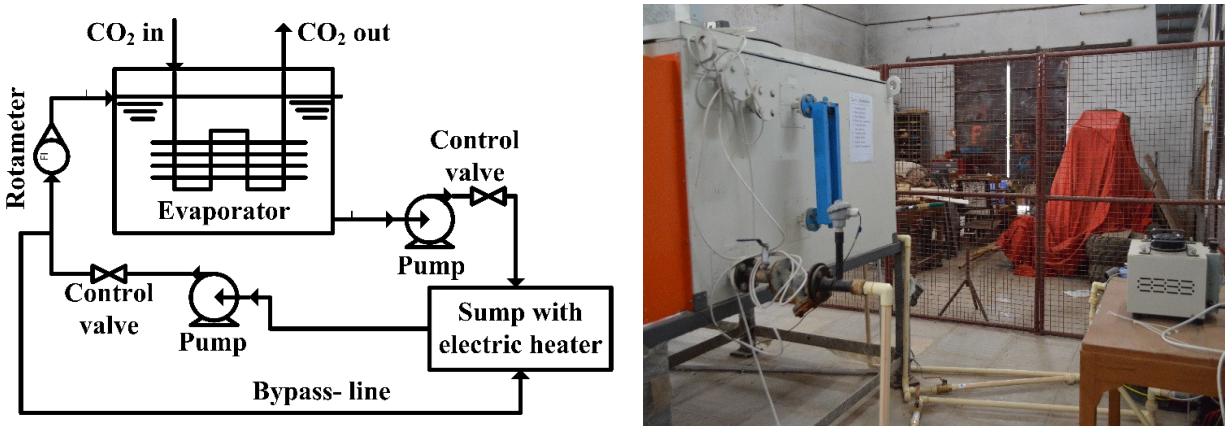

Fig. 4.11 Chiller load simulator

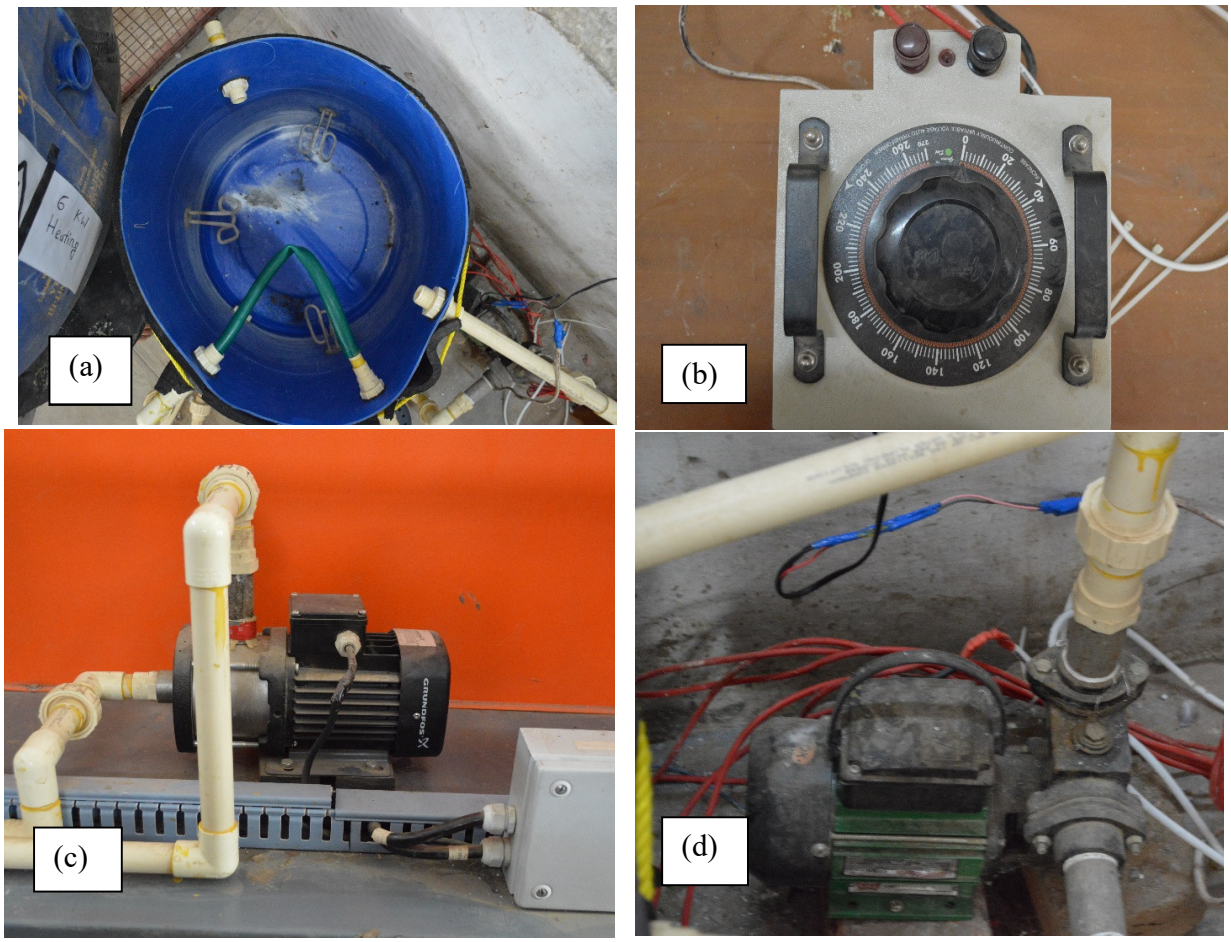

Fig. 4.12 Evaporator load simulator parts, (a) Heaters, (b) Autotransformer, (c) Pump at suction end and (d) Pump at delivery end.

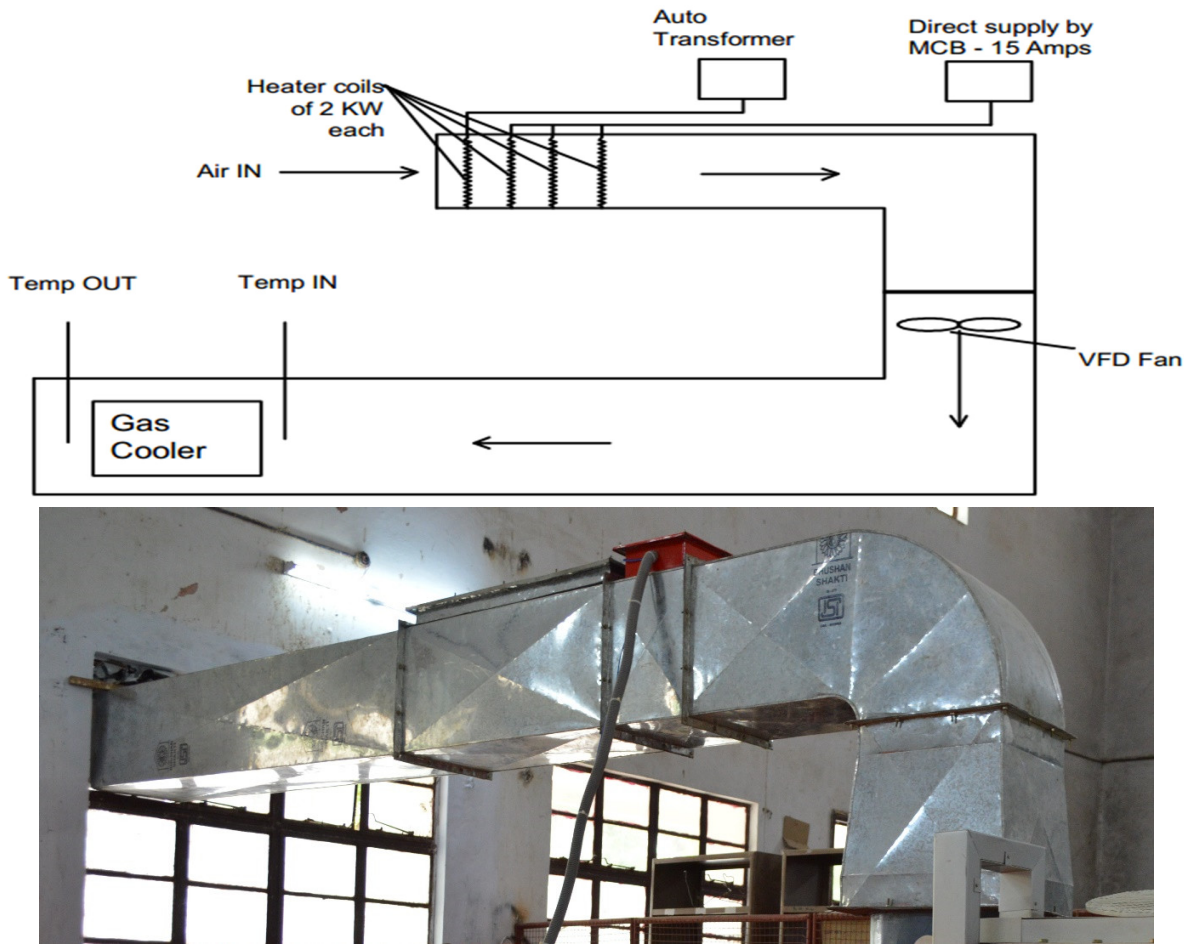

Fig. 4.13 Ambient load simulator

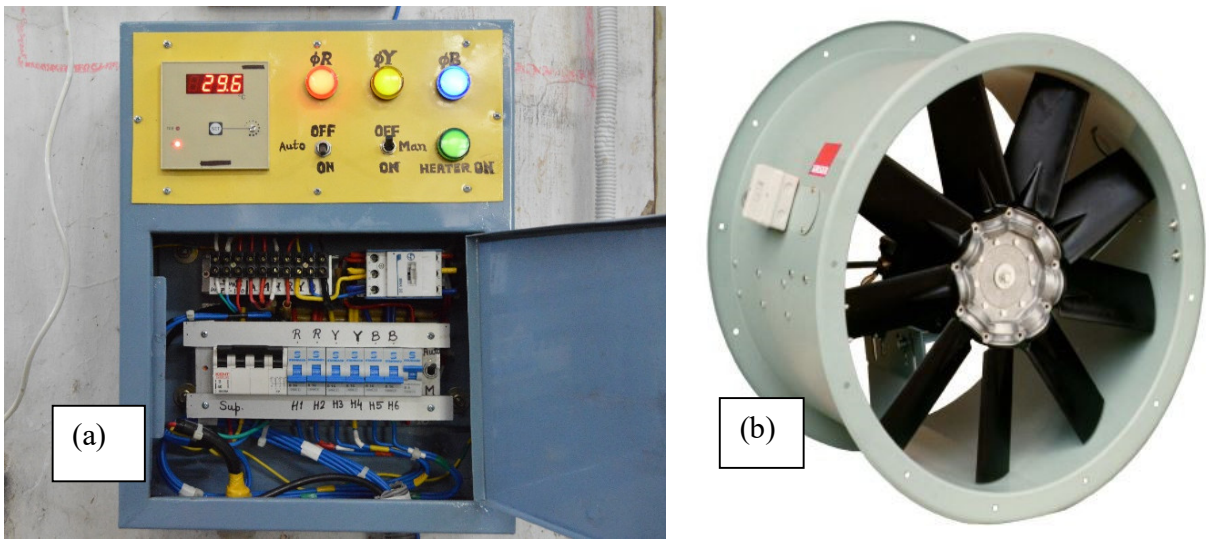

Fig. 4.14 (a) Automatic controller for ambient simulator and (b) VFD axial fan

4.1.10 Instrumentation

The experimental facility is instrumented to digitally record the required measurable quantities, like temperature (RTD, shown in Fig. 4.15 a) and pressure at inlet and outlet of each component (transducer: piezo electric, shown in Fig. 4.15 b), volume flow rate of refrigerant (turbine flowmeter, shown in Fig. 4.15 c) as well as secondary fluid (rotameter, shown in Fig. 4.15 d), compressor power consumption and fan power consumption (energy meters, shown in Fig 4.15 e). The density of refrigerant is estimated based on the compressor suction temperature. The type make and rated accuracy of all the measuring sensors and instruments are given in Table 4.5.

Table 4.5 Accuracies of measuring sensors and instruments

Measurable quantity	Type of device	Quantity	Accuracy
Temperature (°C)	RTD PT 100	8	±0.2°C
Temperature (°C)	RTD PT 100	6	±2°C*
Pressure (bar)	Pressure transducer	8	±2 (bar)
CO_2 flow rate (lpm)	Turbine flow meter	1	±0.5% of reading
Secondary fluid flow rate (lpm)	Rotameter	1	±0.1% of reading
Compressor power (kW)	Digital energy meter	1	±0.5% of reading
Fan power (W)	Digital energy meter	1	±0.5% of reading

**For system monitoring*

4.2 Test procedure

The tests on CO_2 refrigeration system (chiller) are conducted following the guidelines of ARI standard 550/590 (ARI, 2003), maintaining 35°C as ambient Dry Bulb Temperature (DBT) and 5°C temperature difference across the solution (water/glycol; 50:50) circulating in chiller. Further, the tests are also extended for off-design conditions, keeping the ambient DBT lower (32°C) and higher (40°C & 45°C) the design condition (35°C). In all the experiments, the degree of superheat at the evaporator outlet is fixed at 10°C and the compressor speed at 1450 rpm.

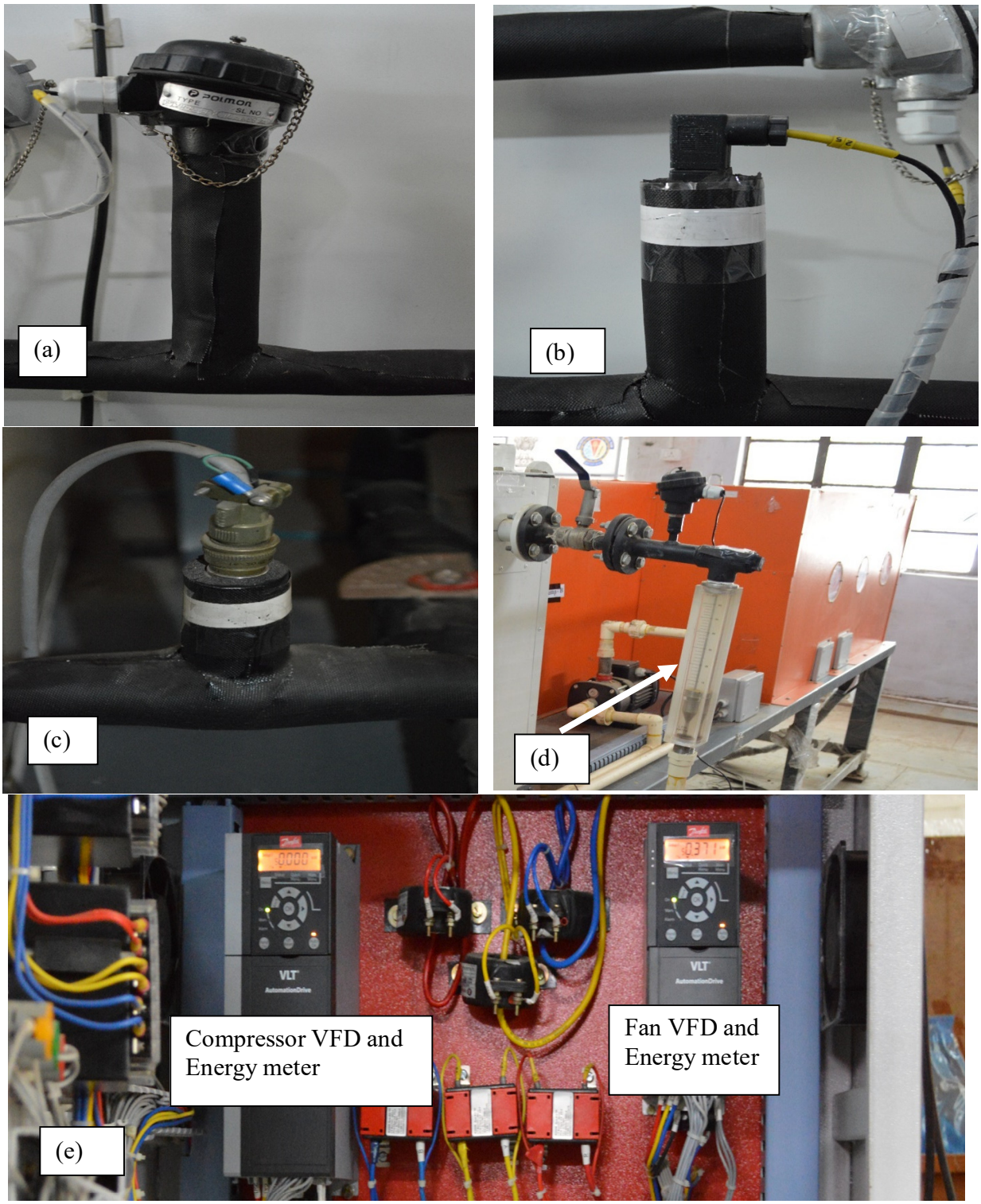

Fig. 4.15 Instrumentation, (a) RTD, (b) Pressure transducer, (c) Turbine flow meter, (d) Rotameter, and (e) Energy meters

The auxiliary systems are first turned on and set to the desired test condition. For evaporator load simulator, the mass flow rate as well as the temperature of circulating solution is set and recorded manually. While for ambient simulator, the DBT of ambient air as well as air velocity over the gas cooler is pre-set. After that the compressor is switched on and subsequently, the performance of system is recorded using data acquisition system (DAQ, shown in Fig. 4.16). The steady state was identified in approximately 35 min of experimental run ensuring maximum permissible pressure deviation of ±0.3 bar for all pressure sensors, ±2°C for temperature sensors, except for the gas cooler outlet temperature sensor for which temperature deviation of ±0.2°C only was allowed. With the help of bypass valve settings, the experiments are conducted with and without IHX as per plan and performances are compared under similar working conditions. Experimental readings are presented in Appendix A.

Fig. 4.16 Data acquisition system (DAQ, POLMON PL 160)

4.3 Data reduction

The data reduction scheme for estimation of the derived quantities such as refrigeration capacity, COP, effectiveness of IHX, exergy destruction and second law efficiency are discussed in this section. The thermo-physical properties of air and the water-glycol mixture are estimated based on the average temperature using the polynomials from the ASHRAE Handbook

(Handbook, 2014). While, the properties of CO_2 are calculated using Refprop (Lemmon et al., 2002).

The effective refrigeration capacity for the system is calculated using the energy balance across the inlet and outlet state of the secondary fluid, using equation (4.1). The same is validated using the experimentally obtained refrigerant side state points at inlet and outlet of the evaporator and the mass flow rate of the refrigerant, as in equation (4.2).

$$RE_s = \rho_s \cdot \dot{\omega}_s \cdot c_{p,s} \cdot \left(T_{s,in} - T_{s,out}\right) \tag{4.1}$$

$$RE_r = \rho_r \cdot \dot{\omega}_r \cdot \left(h_{r,out} - \dot{h}_{r,in}\right)_e \tag{4.2}$$

COP is defined as the ratio of refrigeration capacity to the total power consumption and is calculated using equation (4.3).

$$COP = \frac{RE_s}{\left(\dot{W}_c + \dot{W}_f\right)} \tag{4.3}$$

The effectiveness of IHX is defined as the ratio of actual heat transfer rate ($\dot{Q}_{IHX}$) to the thermodynamically possible maximum heat transfer rate ($\dot{Q}_{IHX,max}$) (Gosney, 1982). $\dot{Q}_{IHX,max}$ is calculated using equation (4.4) as follows:

$$\dot{Q}_{IHX,max} = \dot{m}_r \cdot \left(h_{LP,out}{}^{*} - h_{LP,in}\right)_{IHX} \tag{4.4}$$

where, $h_{LP,out}{}^{*}$ is calculated based on the measured evaporator pressure and the refrigerant temperature at the IHX inlet in high-pressure side. And $h_{LP,in}$ is calculated at low pressure at the inlet of the IHX. Hence, the effectiveness of IHX is calculated using equation (4.5).

$$\varepsilon = \frac{\dot{Q}_{IHX}}{\dot{Q}_{IHX,max}} = \frac{\left(h_{LP,out} - h_{LP,in}\right)_{IHX}}{\left(h_{LP,out}{}^{*} - h_{LP,in}\right)_{IHX}} \tag{4.5}$$

The exergy losses for the various components in the CO_2 trans-critical system are derived as follows:

Compressor (Tao et al., 2010a)

$$Ex_c = T_{ref} \cdot \dot{m}_r \cdot \left(s_{c,\ out} - s_{c,\ in}\right) \tag{4.6}$$

Gas cooler (Cho and Park, 2016)

$$Ex_{gc} = \dot{m}_r \cdot \left({}^{T_{ref}}\!/_{T_{avg,gc}} \cdot \left(h_{c,\ in} - h_{c,\ out}\right) - T_{ref} \cdot \left(s_{c,\ in} - s_{c,\ out}\right)\right) \tag{4.7}$$

IHX (Tao et al., 2010a)

$$Ex_{IHX} = \dot{m}_r \cdot \left(\left(h_{gc,\ out} - h_{IHX,\ out_{HP}}\right) - T_{ref} \cdot \left(s_{gc,\ out} - s_{IHX,\ out_{HP}}\right)\right) - \dot{m}_r \cdot \left(\left(h_{HX,\ out_{LP}} - h_{e,\ out}\right) - T_{ref} \cdot \left(s_{HX,\ out_{LP}} - s_{e,\ out}\right)\right) \tag{4.8}$$

Expansion valve (Tao et al., 2010a)

$$Ex_{exp} = T_{ref} \cdot \dot{m}_r \cdot \left(s_{exp,\ out} - s_{exp,\ in}\right) \tag{4.9}$$

Evaporator (Cho and Park, 2016)

$$Ex_e = \dot{m}_r \cdot \left(\left({}^{T_{ref}}\!/_{T_{avg,e}} \cdot \left(h_{e,\ in} - h_{e,\ out}\right)\right) - T_{ref} \cdot \left(s_{e,\ in} - s_{e,\ out}\right)\right) \tag{4.10}$$

$T_{avg,gc}$ and $T_{avg,e}$ are the external fluid thermodynamic average temperature for gas cooler side and evaporator side, respectively (Sarkar et al., 2004). The thermodynamic average temperatures are calculated using the expressions as shown in equation (4.11) and equation (4.12).

$$T_{avg,gc} = T_{a,out} - T_{a,in} ln\left({}^{T_{a,out}}\!/_{T_{a,in}}\right) \tag{4.11}$$

$$T_{avg,e} = T_{s,in} - T_{s,out} ln\left({}^{T_{s,in}}\!/_{T_{s,out}}\right) \tag{4.12}$$

Where, subscript "a" denotes air at gas cooler side and "s" denotes secondary fluid at evaporator side. The total exergy loss/destruction for the system with and without IHX are given respectively by equation (4.13) and equation (4.14).

$$Ex_{total,\ basic} = Ex_c + Ex_{gc} + Ex_{exp} + Ex_e \tag{4.13}$$

$$Ex_{total,\ IHX} = Ex_c + Ex_{gc} + Ex_{IHX} + Ex_{exp} + Ex_e \quad (4.14)$$

The exergy efficiency for the system with and without IHX are given by equation (4.15) and equation (4.16).

$$\eta_{second,\ basic} = 1 - \left(\frac{Ex_{total,\ basic}}{\dot{W}_c}\right) \quad (4.15)$$

$$\eta_{second,\ IHX} = 1 - \left(\frac{Ex_{total,\ IHX}}{\dot{W}_c}\right) \quad (4.16)$$

And, the irreversibility contribution of the components is estimated using equation (4.17).

$$\delta_{component} = \frac{Ex_{component}}{Ex_{total}} \quad (4.17)$$

4.4 Uncertainty analysis

A method for estimating uncertainty in derived quantities as suggested by Moffat (1985) is followed for assessing the accuracy of mass flow rate of refrigerant. The function J is expressed as in equation (4.18).

$$J = f(u_1, u_2, u_3, \dots\dots, u_N) \quad (4.18)$$

where, u_k are the measured quantities and J is the derived quantity. The uncertainty of the derived quantity J owing to the uncertainties in each u_k is determined as root-sum-square, as in equation (4.19). Using the uncertainties of the measured quantities that are refrigerant volume flow rate and compressor suction pressure and temperature, the resulting accuracy in prediction of mass flow rate of refrigerant is found to be 1.8%.

$$\Delta J = \sqrt{\sum_{k=1}^{N} \left(\frac{\partial J}{\partial u_k} \partial x_k\right)^2} \quad (4.19)$$

For the other measured quantities, which are refrigeration effect, COP, IHX effectiveness and exergy efficiency, a method suggested by Lindberg (2000) is adopted, as calculation of these measured quantities involves enthalpy/entropy values and which cannot be determined explicitly. Uncertainty in enthalpy/entropy is calculated as maximum within the bounds of uncertainty in recording of pressure and temperature. Computed uncertainty in refrigeration effect (calculated using Eq. 4.1), refrigeration effect (calculated using Eq. 4.2), COP, IHX effectiveness and exergy efficiency are found to be ±3.7%, ±3.1%, ±3.6%, ±2.9% and ±3.4%, respectively.

4.5 Results and discussions

In this section, performance comparison of a CO_2 refrigeration system equipped with and without IHX is presented from the energetic and exergetic perspectives. To validate the experimentally, obtained value of refrigerant capacity, heat transfer balance is conducted between the secondary fluid side and the refrigerant side across the evaporator. The results from the same is plotted in Fig. 4.17. The maximum deviation in energy balance for the evaporator is found to be ±10.95%, while the minimum deviation recorded is as ±1.73%. Hence, the experimental results are considered reliable for analysis and conclusion.

4.5.1 Compressor inlet temperature and refrigerant mass flow rate

Adoption of IHX leads to increase in refrigerant temperature at compressor suction, which results into reduction of specific volume of refrigerant at the compressor suction. This leads to reduction in mass flow rate and increment in specific compressor work ($kJ \cdot kg^{-1}$). Owing to these two contradictory effects, compressor power requirement (kW) for IHX cycle is nearly equal or marginally higher than the basic cycle and it depends strongly on the operating parameters. Further, adoption of IHX tends to increase specific refrigeration capacity ($kJ \cdot kg^{-1}$),

however, due to reduction in mass flow rate, the refrigeration capacity (kW) may decrease or increase, depending on ambient temperature and gas cooler pressure.

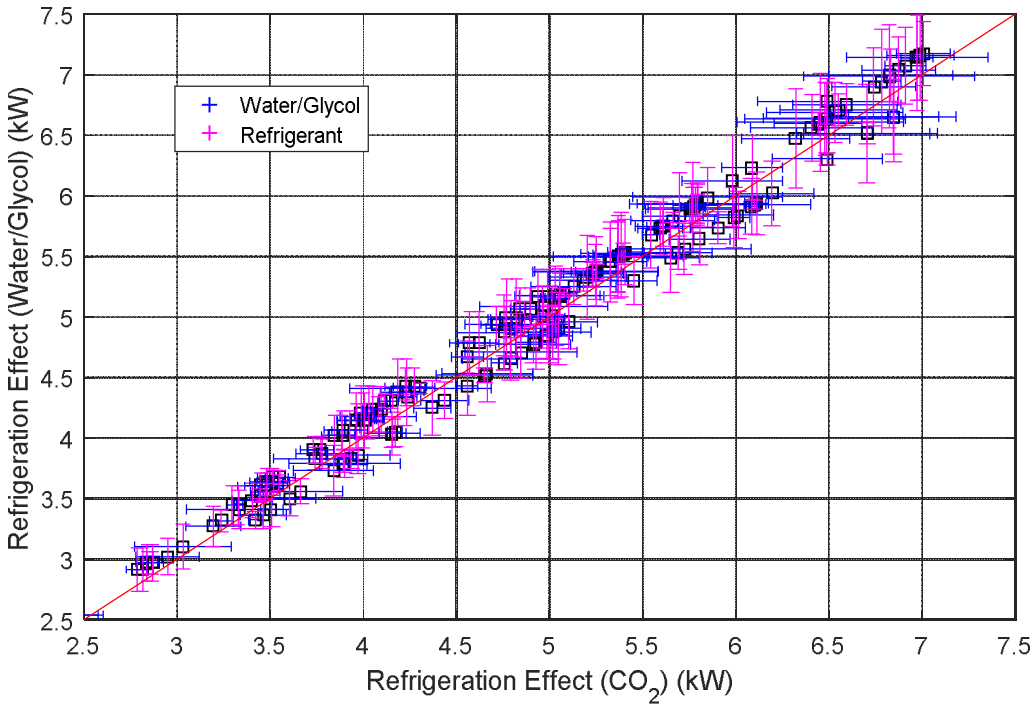

Fig. 4.17 Energy balance deviation for the evaporator

The experimentally recorded compressor inlet temperature and mass flow rate for the CO_2 system with and without IHX for various operating conditions at air flow velocity 1 $m \cdot s^{-1}$, are represented in Fig. 4.18 and Fig. 4.19, respectively. As expected, referring Fig. 4.18, the compressor inlet temperature is found comparatively higher for cycle with IHX. Further, it increases with increase in ambient condition. It is observed from the Fig. 4.19 that with increase in compressor discharge pressure (i.e. compression ratio), the mas flow rate of the refrigerant decrease, irrespective of the evaporator temperature for both cases with and without IHX. This may be attributed to the reduction of compressor volumetric efficiency with increase in compression ratio. With increase in evaporator temperature, the mass flow rate, for both systems increase due to decrease in specific volume. The mass flow rate in IHX system is found to be lower than that in basic system, which is due to the increased specific volume for the IHX cycle.

The mass flow rate of IHX system further reduces with increase in ambient temperature, owing to the increase in refrigerant temperature at the outlet of IHX in the low-pressure side. Maximum reduction of the mass flow rate in IHX system for 45ºC ambient condition is found to be 11.2% for -5ºC evaporator temperature and 10.3% for 0ºC evaporator temperature.

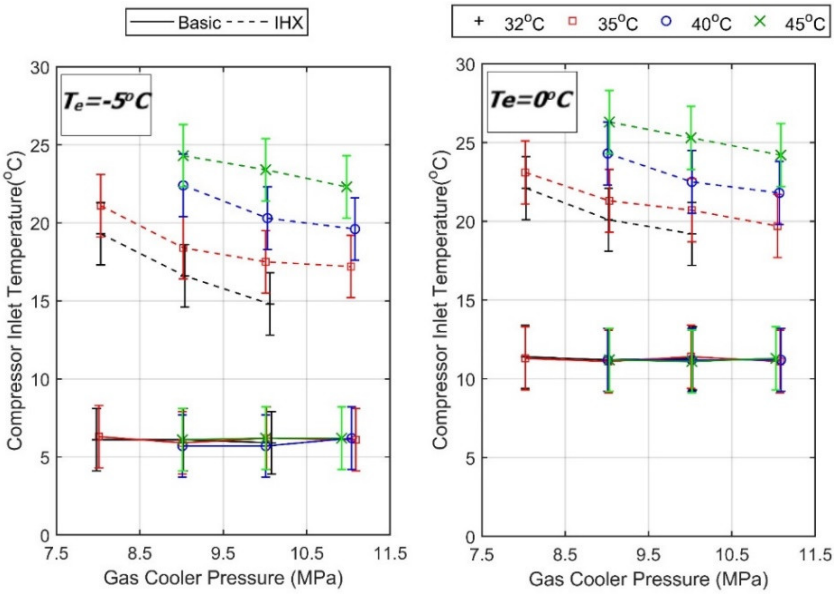

Fig. 4.18 Compressor inlet temperature for various operating conditions

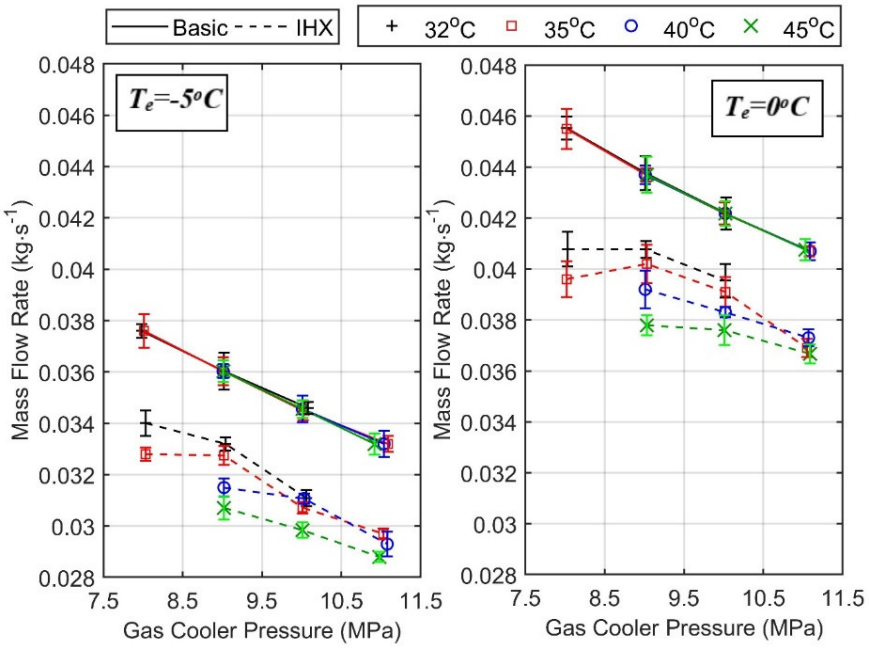

Fig. 4.19 Refrigerant mass flow rate for various operating conditions

4.5.2 Effectiveness of IHX

Fig. 4.20 presents the computed value of effectiveness of IHX for the tested operating range, which is found variable. It is to be noted that, in literature, many of the theoretical studies considered the effectiveness of IHX as a constant value. Variable nature of effectiveness of IHX is also reported in the experimental conducted by Torrella et al., (2011).

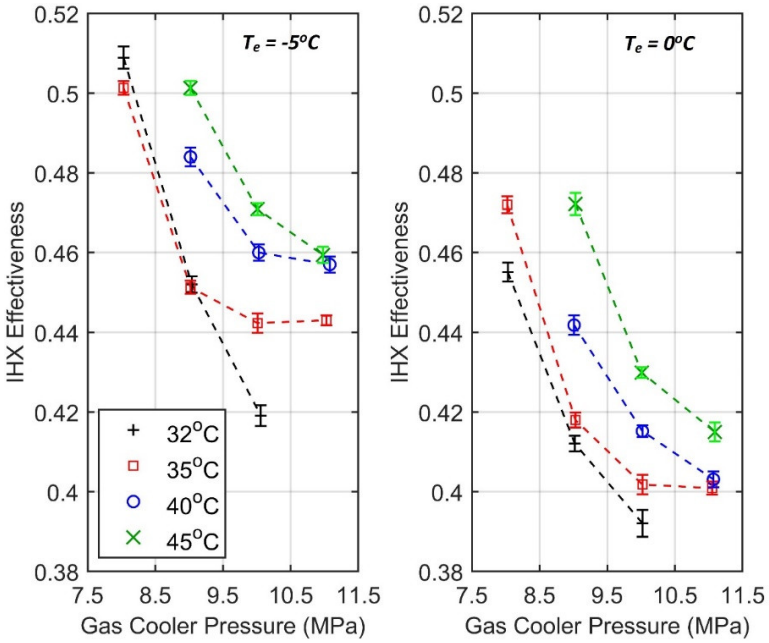

Fig. 4.20 IHX effectiveness for various operating conditions

It is also observable from the Fig. 4.20 that the effectiveness of IHX decrease with increase in compressor discharge pressure and evaporator pressure. This is due to the prominent variation of isobaric heat capacity of the refrigerant, which decrease with increase in compression ratio. In other words, owing to the influence of operating pressure on isobaric heat capacity, high reheating of refrigerant is required at the low-pressure side for achieving meaningful sub-cooling of the refrigerant at the high-pressure gas cooler side. Further, the IHX effectiveness increase with increase in ambient temperature due to the increase in refrigerant temperature at the entry of IHX in the high-pressure side. For evaporator temperature of 0°C, the

derived IHX effectiveness for the experimental setup is determined to be 0.51 for 45°C ambient temperature and 0.39 for 32°C ambient temperature.

4.5.3 Compressor discharge temperature

The performance of compressor is found to be strongly related to the refrigerant suction temperature and the compression ratio. Adoption of IHX is observed to lead to superheating of the refrigerant vapor, which considerably increases the compressor discharge temperature. The increase of compressor discharge temperature and pressure, may lead to degradation of the lubricant oil, reduction of compressor life and a decrement in the compressor isentropic efficiency. Fig. 4.21 shows the effect of various operating parameters on the compressor discharge temperature for both basic cycle and IHX cycle.

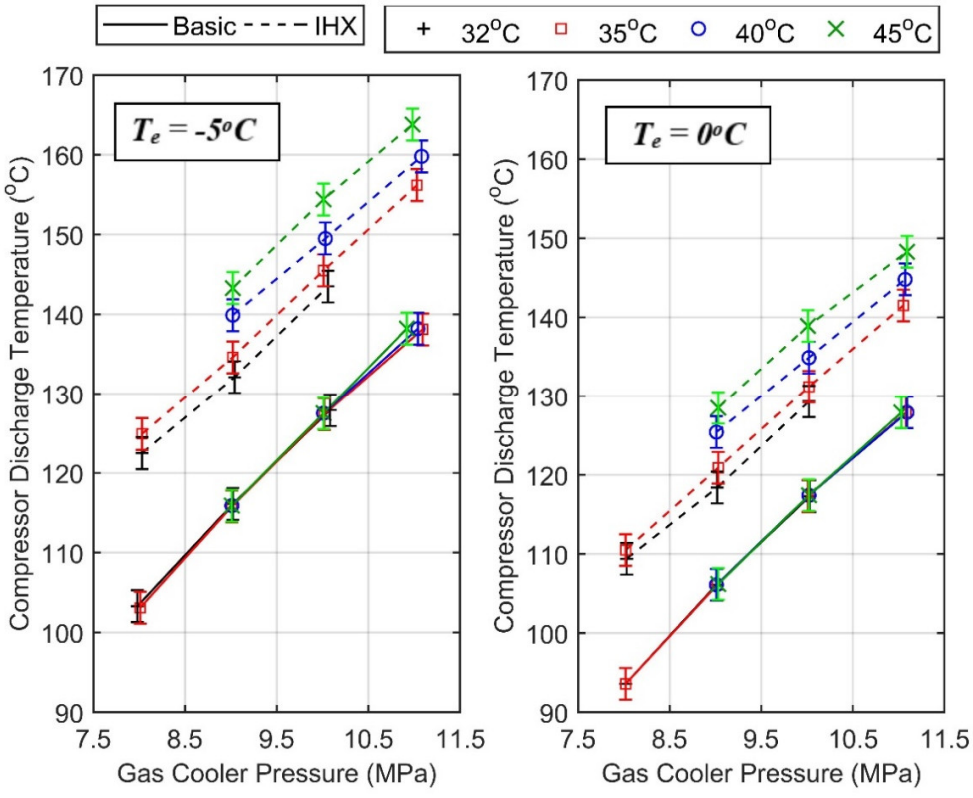

Fig. 4.21 Compressor discharge temperature for various operating conditions

It is observable from the Fig. 4.21 that with increase in compressor discharge pressure, the discharge temperature increases and the same increment is higher for the IHX cycle, especially for high ambient condition. The maximum rise recorded in compressor discharge temperature is about 24ºC which was observed at -5ºC evaporator temperature for 45ºC ambient.

4.5.4 Energetic parameters

Fig. 4.22 and Fig. 4.23 presents experimental result of effect of change in ambient temperature on some of the prominent energetic parameters namely, compressor power, refrigeration capacity and COP, for a wide range of gas cooler pressure. It is observed that refrigeration capacity for both cycles (with and without IHX), increase with increase in gas cooler pressure, while the rate of increment increases up to a certain optimal pressure value corresponding to the ambient temperature and beyond the optimum the rate reduces. For example, at ambient temperature of 35ºC, the refrigeration effect increases sharply up to 90 bar (for the range of gas cooler pressure investigated) but beyond this pressure, the rate of increment reduces. Whereas, the compressor power consumption is found to steadily increase with the increase in compressor pressure. Hence, there is a need to optimize gas cooler pressure to attain best possible COP corresponding to the ambient condition. These results are found consistent with the reported in literature.

The refrigeration effect for most of the experimental data points for IHX cycle is found higher while, the compressor power is found nearly similar for both the cycles, resulting in higher COP for the IHX cycle. It is worth mentioning that the improvement in refrigeration capacity for IHX cycle is found higher near the critical pressure i.e. at 80 bar. This is due to the typical ‘S’ form of isothermal lines, where large increments in specific cooling capacity is possible even with a small decrease in refrigerant temperature.

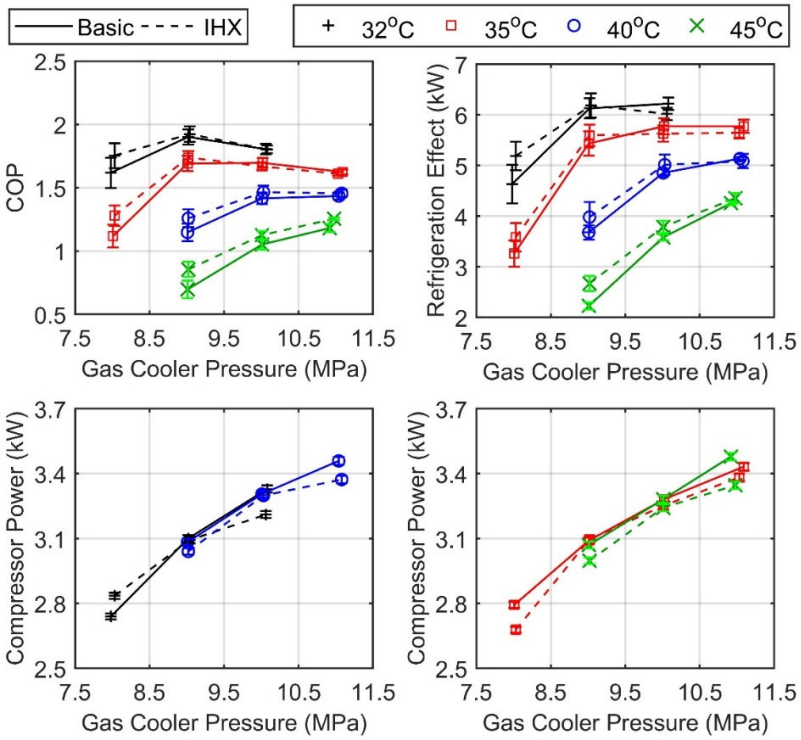

Fig. 4.22 Effect of ambient temperature on the energetic parameters (T_e = -5°C)

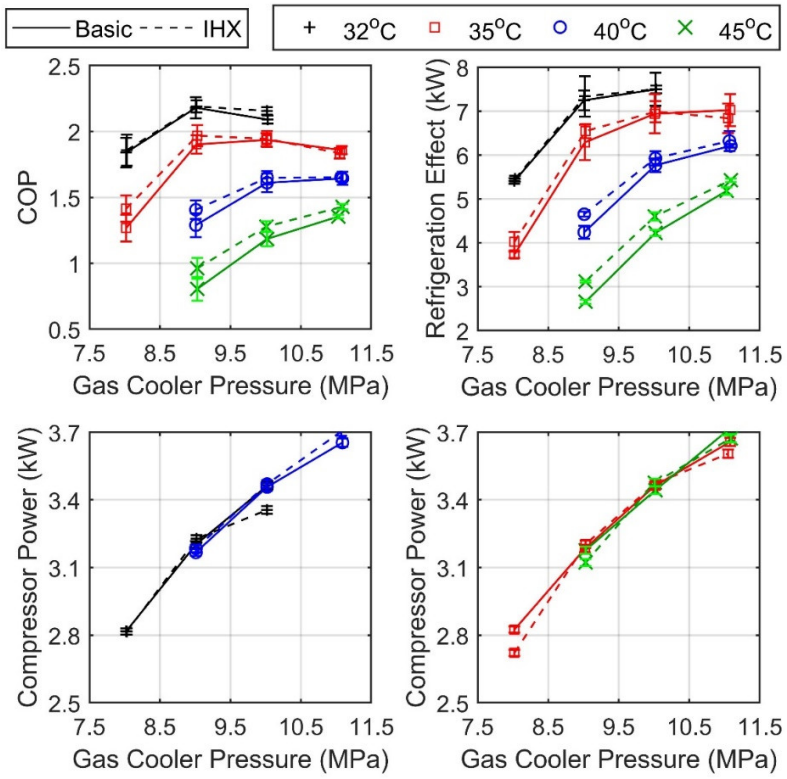

Fig. 4.23 Effect of ambient temperature on the energetic parameters (T_e = 0°C)

The improvement in COP for IHX cycle is found to increase with increase in ambient temperature as observable in Fig. 4.22 and Fig. 4.23. Further, as expected, the extent of improvement increases with decrease in evaporator temperature. Moreover, IHX cycle can be operated at comparatively lower gas cooler pressure than the basic cycle, for the best possible COP. This is concluded from the observation that even at lower gas cooler pressure than the optimal, the COP as well as refrigeration effect are higher for the IHX cycle. While, at a gas cooler pressure higher than the optimal pressure, the COP of IHX cycle is observed to be similar or even lower than the basic cycle.

The performance of gas cooler is sensitive to the velocity of the air flowing across the tube banks (Gupta and Dasgupta, 2014; Li et al., 2017; Li, 2013; Li et al; 2012). In, general with increase in air velocity over the gas cooler, the overall heat transfer coefficient improves, which leads to reduction in approach temperature (difference between the refrigerant temperature at gas cooler outlet and the ambient temperature). On the other hand, the fan power consumption, increase. This may lead to reduction in COP. Hence, it is important to investigate the best possible air flow velocity over gas cooler, which of course is a compromise between the specific cooling capacity and fan power consumption.

Fig. 4.24 presents the experimentally recorded fan power and the fan efficiency for various air flow velocities. The fan power and the fan efficiency varies from 21.89 (W) to 334.28 (W) and 58.49% to 46.07%, respectively, for the range of air velocity (1 $m \cdot s^{-1}$- 3 $m \cdot s^{-1}$) investigated.

Fig. 4.25 and Fig. 4.26 are plotted taking gas cooler pressure in the x-axis and the energetic parameter (approach temperature and COP) in the y-axis, for three air flow velocities (1 $m \cdot s^{-1}$, 2 $m \cdot s^{-1}$ and 3 $m \cdot s^{-1}$), at evaporator temperature -5^{o}C. It is observable from the Fig. 4.25

that with increase in air side velocity over the gas cooler, the approach temperature tends to reduce, both for basic as well as IHX cycle, irrespective to the ambient temperature. Inspite of reduction in approach temperature, the COP is found to have a decreasing tendency (Fig. 4.26). The variation of approach temperature with respect to evaporator temperature is not found significant, hence not shown here. With increase in gas cooler pressure, for most experimental readings, the approach temperature is observed to reduce. However, for a fewer data sets, the approach temperature has also been observed to increase with increase in gas cooler pressure for short interval near the critical pressure 80-90 bar. This may be attributed to rapid change of CO_2 properties near the critical zone.

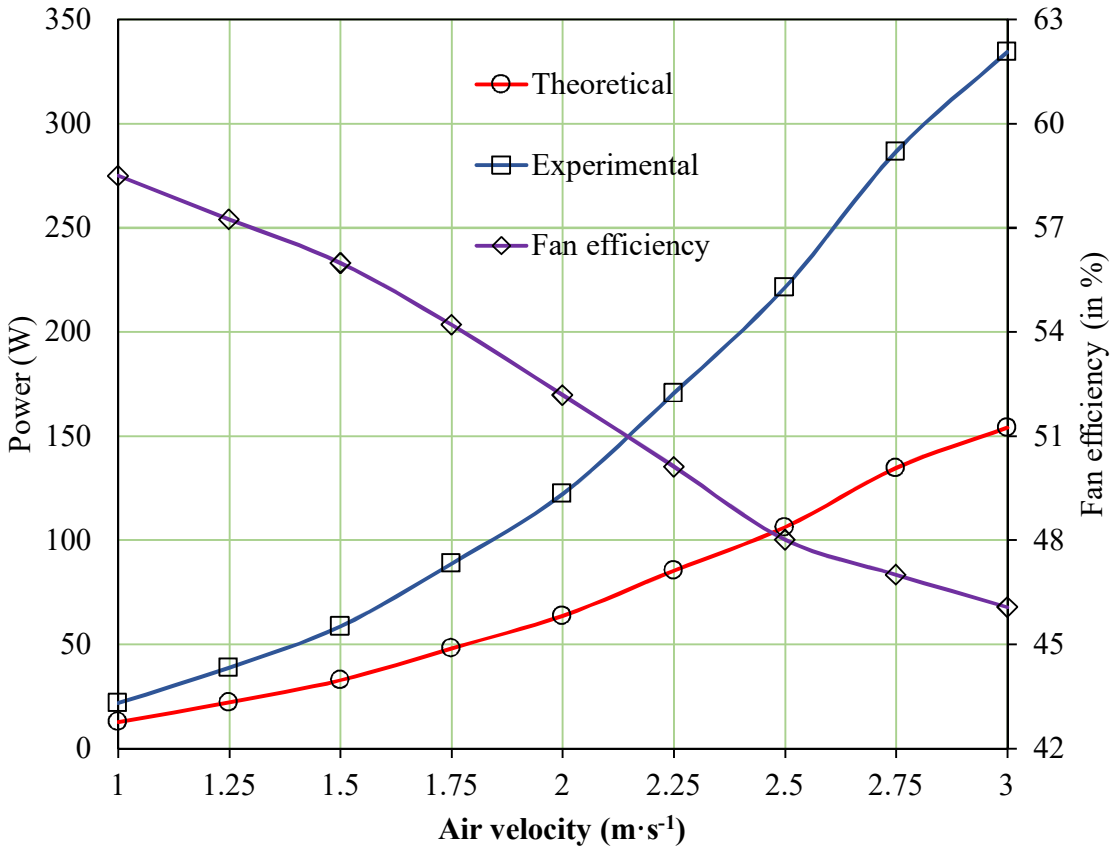

Fig. 4.24 Fan power and fan efficiency for the range of experiments

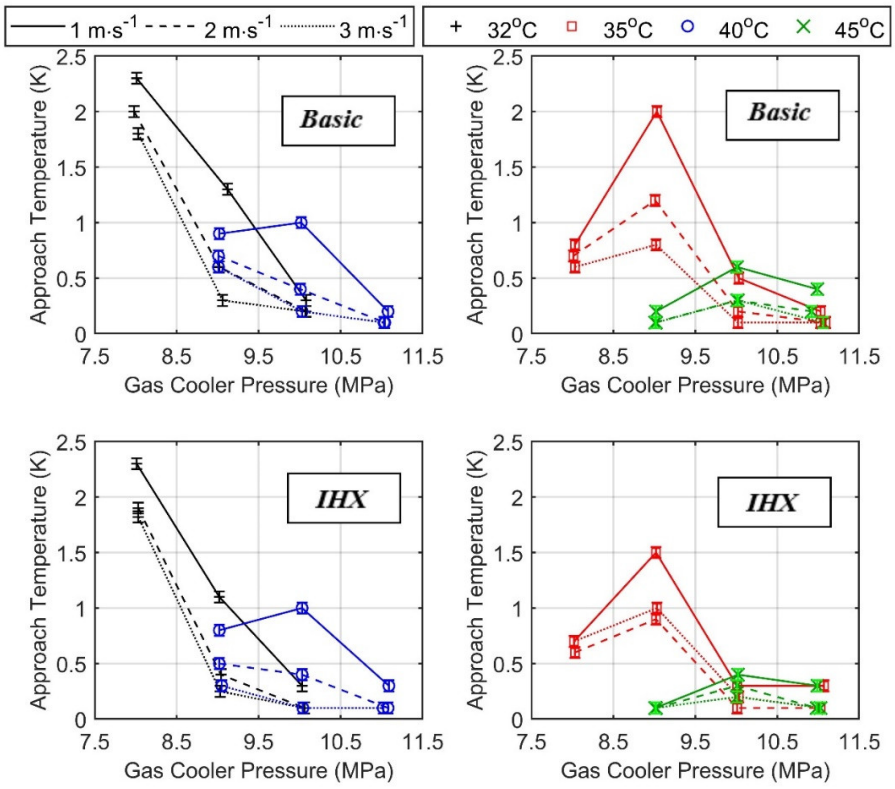

Fig. 4.25 Effect of gas cooler side air velocity on approach temperature

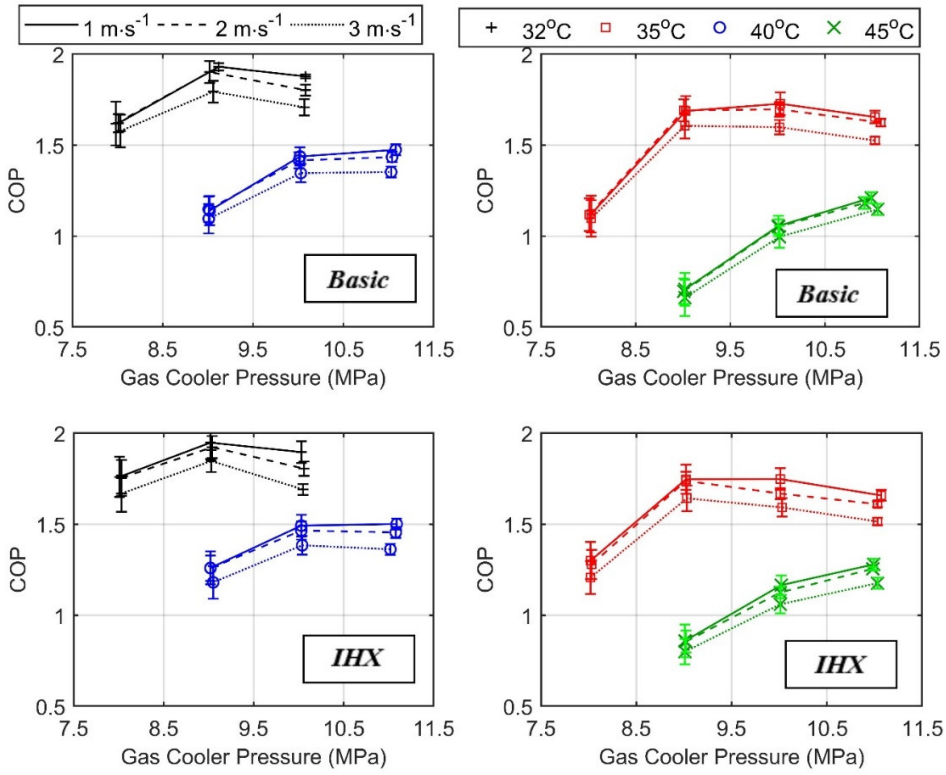

Fig. 4.26 Effect of gas cooler side air velocity on COP

For basic cycle, within ambient temperature of 32ºC & 45ºC, the best possible COP corresponding to the air flow velocity of 1 $m \cdot s^{-1}$, 2 $m \cdot s^{-1}$ and 3 $m \cdot s^{-1}$ are recorded within range 2.19 to 1.35, 2.18 to 1.34 and 2.05 to 1.31, respectively. Whereas, within same ambient temperature and air velocity range, the COP for IHX cycle are recorded to be within marginally higher range of 2.20 to 1.43, 2.19 to 1.42 and 2.06 to 1.32. For the present geometry of the gas cooler and the fan setup, the overall energy efficiency obtained is maximum at lower air velocity. Literature on experimental investigation on effect of fan power consumption on COP is scarce but it is found to be important, so further investigation is carried out.

The sensitivity of fan efficiency on fan power and ultimately, on COP of the cycle is presented in Table 4.6. Sensitivity analysis is conducted for both cycles with and without IHX, operating at two ambient temperatures (32ºC & 45ºC) for one evaporating temperature setting of 0ºC. As observable, with increase in fan efficiency there is no substantial change in the optimal air flow velocity. However, with increment in fan efficiency, there is reduction in fan power leading to improvement in COP is observed. The improvement in COP is found more prominent at higher air flow velocity, which is expected, as the fan power varies exponentially with air velocity. A maximum of 3.73% improvement in COP is attainable at air flow velocity of 3 $m \cdot s^{-1}$, if the fan efficiency is 75%. It is important to note that near the optimal air velocity of 1 $m \cdot s^{-1}$, the maximum improvement in COP is found to be only 0.152% at 75% fan efficiency. This implies, there is tangible scope of high efficiency-high speed fan for overall cycle efficiency improvement at high ambient.

Fig. 4.27 summarizes the overall improvement in performance of IHX over the basic cycle in terms of COP, keeping the air velocity 1 $m \cdot s^{-1}$. At maximum ambient of 45ºC, performance of cycle with IHX is found to lead by about 5.7% for -5ºC evaporator temperature,

while the enhancement is found to be 5.01% for evaporator temperature of 0ºC. The results obtained are found consistent with the findings of Torrella et al., (2011).

Table 4.6 Sensitivity of fan efficiency on fan power and COP

(p_{gc} (bar)/T_{amb} (ºC))	Velocity ($m \cdot s^{-1}$)	Fan efficiency	Basic cycle		IHX cycle	
			Fan power (W)	COP (% deviation from experimental)	Fan power (W)	COP (% deviation from experimental)
(90/32)	1	0.58*	21.89	–	21.89	–
		0.55	23.28	-0.044	23.28	-0.043
		0.65	19.72	0.069	19.72	0.068
		0.75	17.07	0.152	17.07	0.149
	2	0.52*	122.24	–	122.24	–
		0.55	115.98	0.188	115.98	0.187
		0.65	98.13	0.730	98.13	0.724
		0.75	85.05	1.131	85.05	1.122
	3	0.46*	334.28	–	334.28	–
		0.55	280.03	1.537	280.03	1.527
		0.65	236.95	2.792	236.95	2.773
		0.75	205.35	3.733	205.35	3.707
(110/45)	1	0.58*	21.89	–	21.89	–
		0.55	23.28	-0.0375	23.28	-0.0372
		0.65	19.72	0.0591	19.72	0.0586
		0.75	17.07	0.130	17.07	0.128
	2	0.52*	122.24	–	122.24	–
		0.55	115.98	0.163	115.98	0.165
		0.65	98.13	0.633	98.13	0.639
		0.75	85.05	0.981	85.05	0.989
	3	0.46*	334.28	–	334.28	–
		0.55	280.03	1.375	280.03	1.386
		0.65	236.95	2.495	236.95	2.516
		0.75	205.35	3.332	205.35	3.604

*Experimental observations

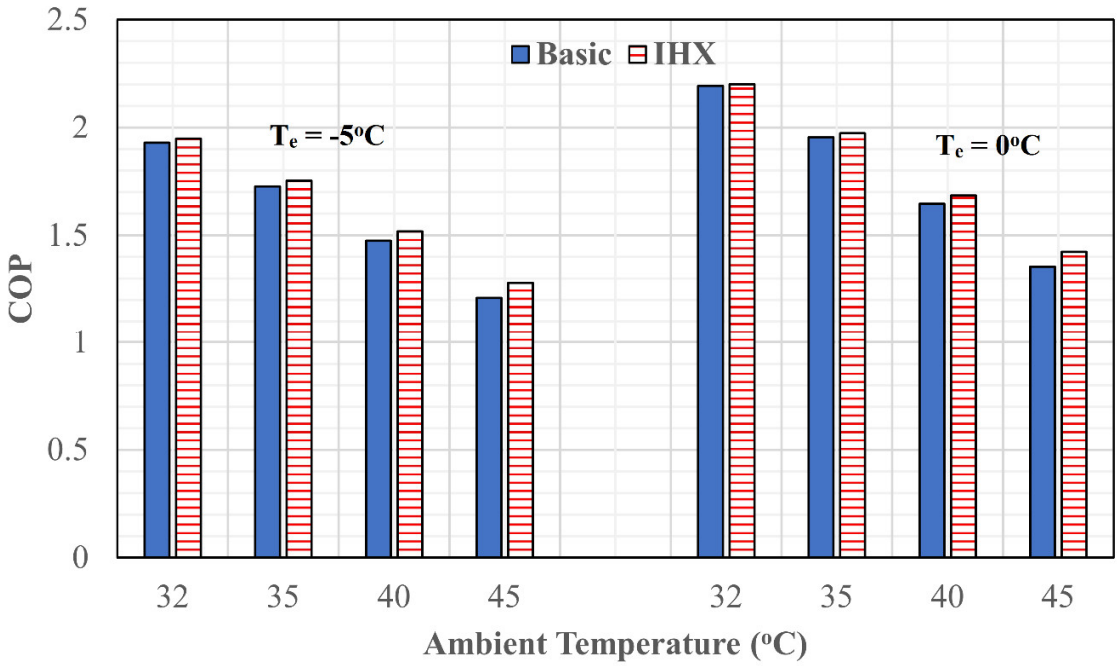

Fig. 4.27 COP and percentage improvement of IHX cycle over the basic cycle

4.5.5 Exergetic parameters

Fig. 4.28 presents the effect of ambient temperature and evaporator temperature on exergetic efficiency of both basic and IHX cycles. With rise in gas cooler pressure, exergetic efficiency tends to increase, reaches a plateau at certain optimal pressure (corresponding to ambient condition) but with further increment in gas cooler pressure, exergetic efficiency decreases. The trend of exergetic efficiency is found like that of energetic efficiency (COP) as seen in Fig. 4.22 and Fig. 4.23. Adoption of IHX leads to improvement in exergetic efficiency and the improvement is found to further enhance with rise in ambient temperature. For both basic and IHX cycles, exergetic efficiency is also found to increase with decrease in evaporator temperature, irrespective of the ambient temperature. At evaporation temperature of -5°C, the improvement in exergetic efficiency for IHX cycle is found to be 3.09% and 5.05% for ambient temperature of 32°C and 45°C, respectively. And, at evaporation temperature of 0°C, the same

improvement is found to be a bit lower at 2.03% and 4.60% respectively, for similar ambient condition.

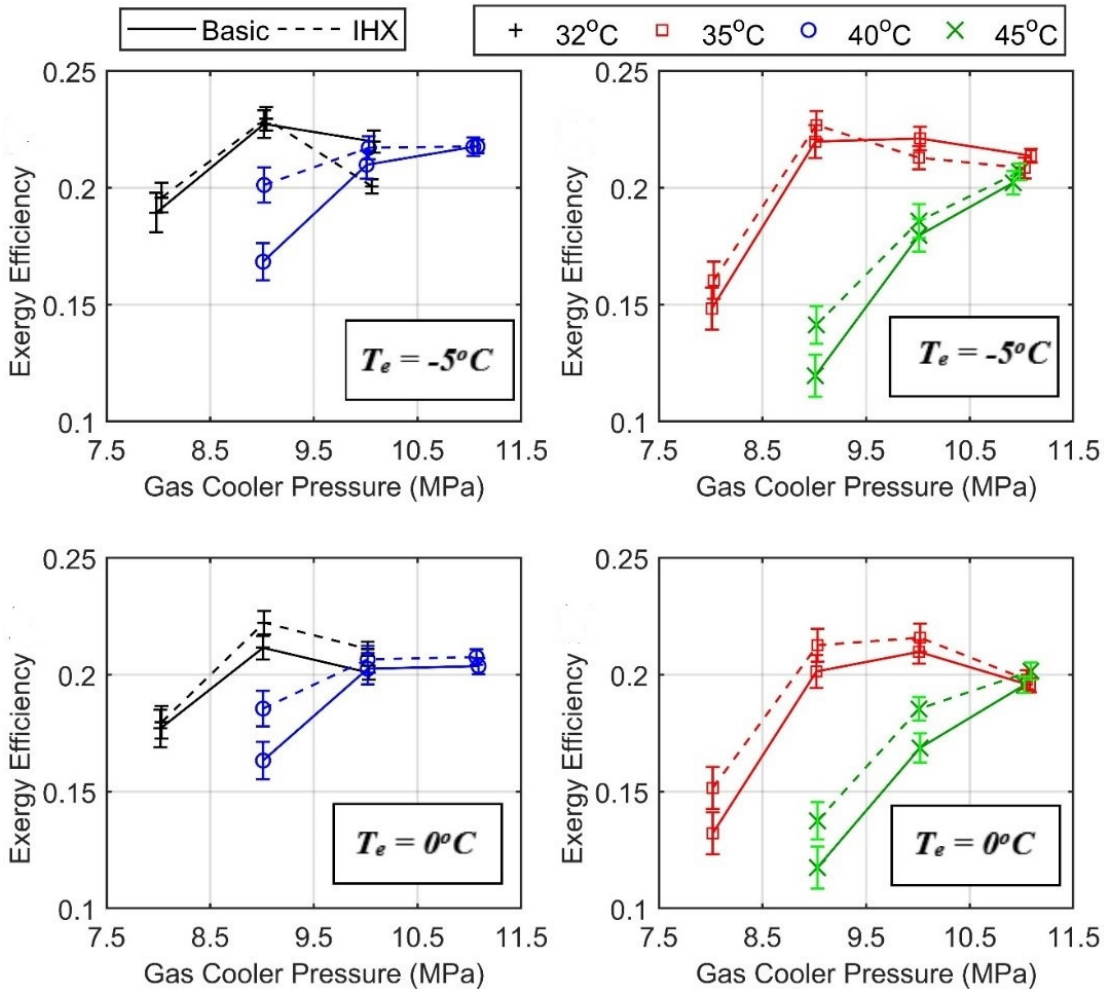

Fig. 4.28 Effect of ambient temperature on the exergetic efficiency

Fig. 4.29 represents effect of ambient temperature on the irreversibility contribution of various components in the chiller system such as compressor, gas cooler and expansion valve at evaporation temperature of 0°C. At lower ambient temperature of 32°C, the gas cooler exhibits the highest percentage of irreversibility among components, while at higher ambient of 45°C, the expansion valve is found to have the highest contribution to system irreversibility. It is also observed that adoption of IHX leads to reduction in compressor's contribution towards system

irreversibility. Significant reduction of exergy loss in expansion valve is also observable from the Fig. 4.29 for the IHX cycle and the same reduction is found to increase with increase in ambient temperature. The effect of evaporation temperature on the irreversibility contribution of compressor, gas cooler and expansion valve are not found to be significant. At ambient temperature of 32°C and air velocity over the gas cooler at 2 $m \cdot s^{-1}$, the maximum contribution of gas cooler towards system irreversibility is found to be 41.6%, while, the contribution of expansion valve at ambient temperature of 45°C is found to be 45.2%.

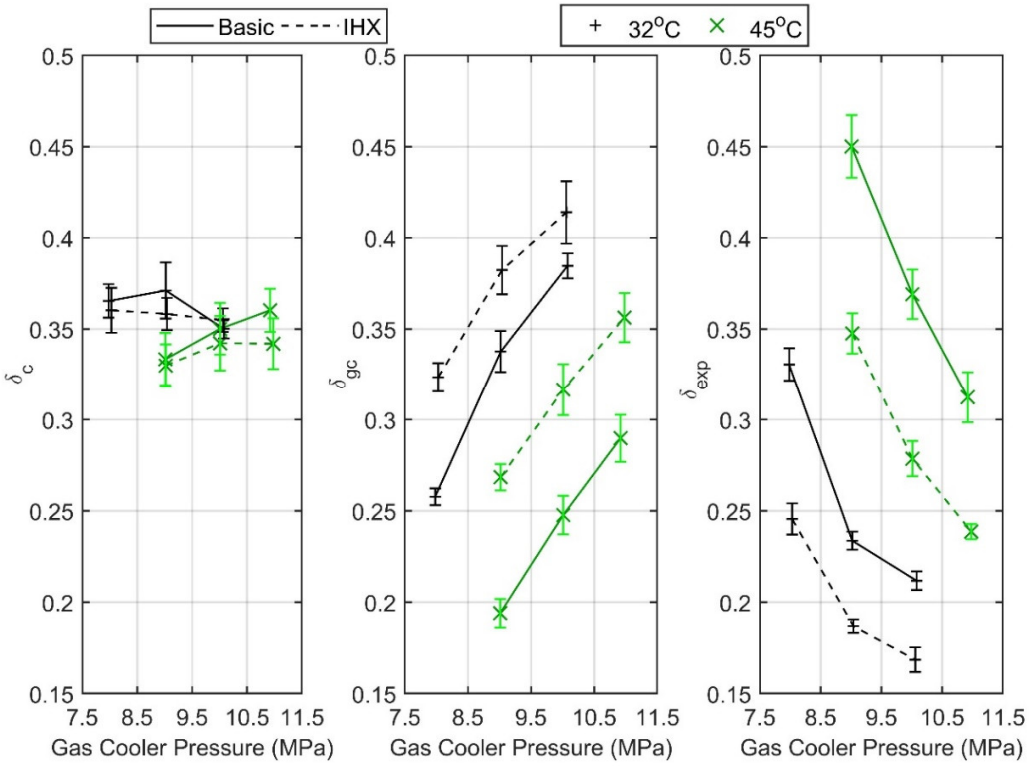

Fig. 4.29 Effect of ambient temperature on the irreversibility contribution of compressor, gas cooler and expansion valve

Fig. 4.30 presents the effect of gas cooler side air velocity on the exergy efficiency at evaporator temperature -5°C. At lower gas cooler pressure and with increase in gas cooler side air velocity, the exergy efficiency tends to increase. While, at higher gas cooler pressure, the exergy efficiency is found to decrease with increase in air velocity. Also, the trend of exergetic

efficiency is found similar to that of energetic efficiency (referring, Fig. 4.25) with respect to gas cooler side air velocity. From the exergetic point of view, the optimal gas cooler side air velocity is found to be near 1 $m \cdot s^{-1}$, which is consistent with the findings from the energetic perspective.

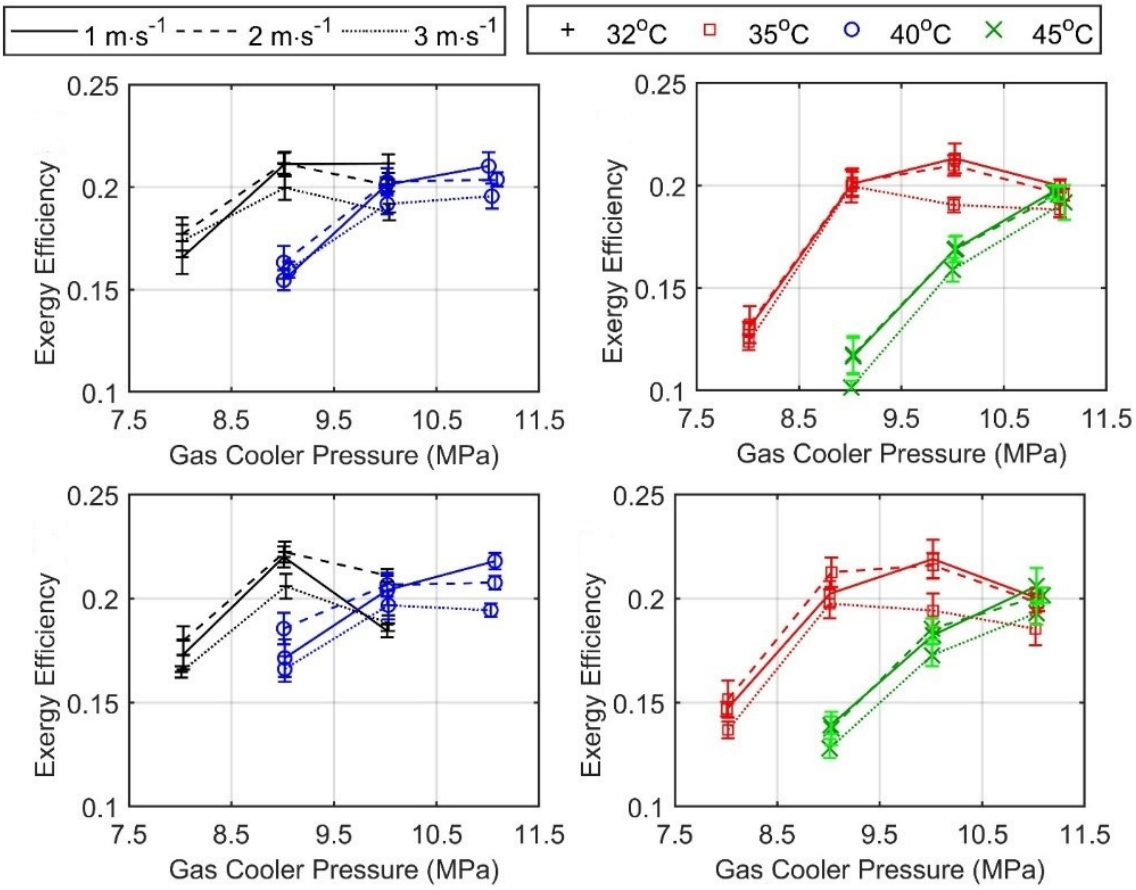

Fig. 4.30 Effect of gas cooler side air velocity on the exergy efficiency

The effect of gas cooler side air velocity on the irreversibility contribution of compressor, gas cooler and expansion valve are represented in Fig. 4.31, at evaporator temperature -5°C. Reduction in irreversibility contribution of compressor and expansion valve are observable, with increment in air velocity. On the other hand, there is increment observed in the irreversibility contribution of gas cooler with increase in air velocity. Owing to these two contradictory effects, there is scope of exploration of optimization for obtaining the best possible exergy efficiency.

Fig. 4.32 represents irreversibility contribution of IHX and evaporator at various ambient temperature, at constant evaporator temperature of -5°C and air velocity of 1 m·s^{-1}. With increase in ambient temperature, the irreversibility contribution of evaporator is found to decrease while, the same for IHX increases. With respect to gas cooler pressure, the irreversibility contribution of evaporator is found to be higher at high ambient. The evaporator contribution towards system irreversibility is found higher for IHX cycle and the irreversibility is found to increase with increase in ambient temperature. Exergy loss contribution of IHX is found to increase with increase in gas cooler pressure, irrespective of the ambient temperature. The effect of evaporation temperature and gas cooler side air velocity on the exergy loss contribution of evaporator and IHX are not found significant and hence not plotted. Among the cycle components, IHX is found to have least contribution towards system irreversibility.

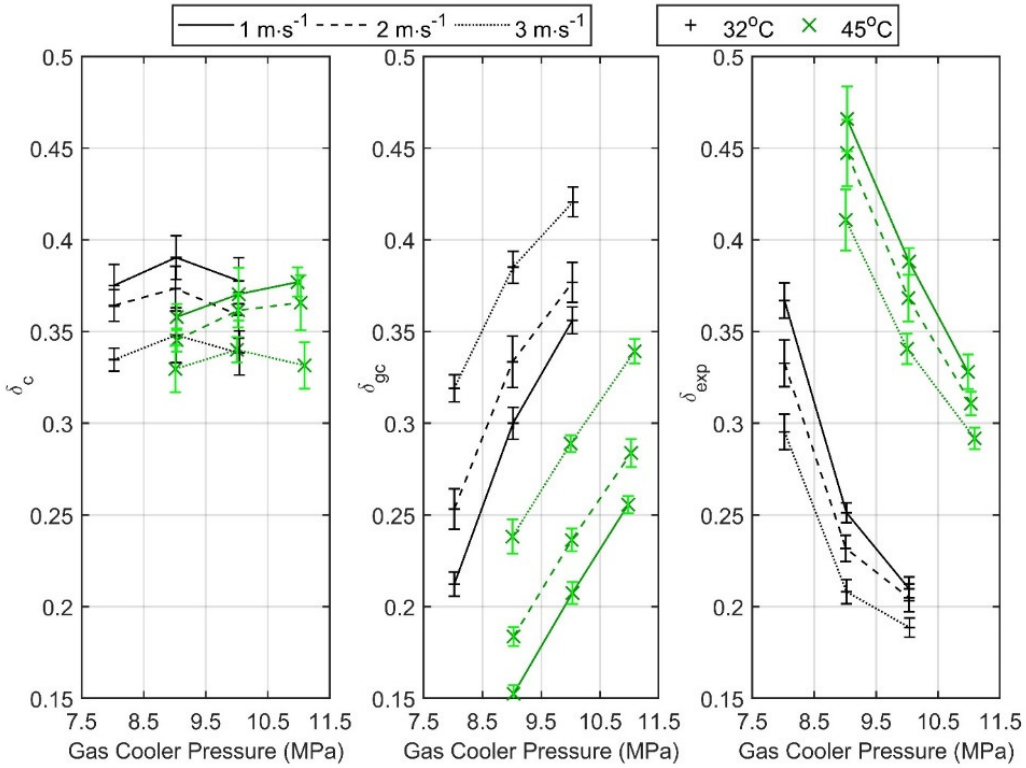

Fig. 4.31 Effect of gas cooler side air velocity on the irreversibility contribution of compressor, gas cooler and expansion valve

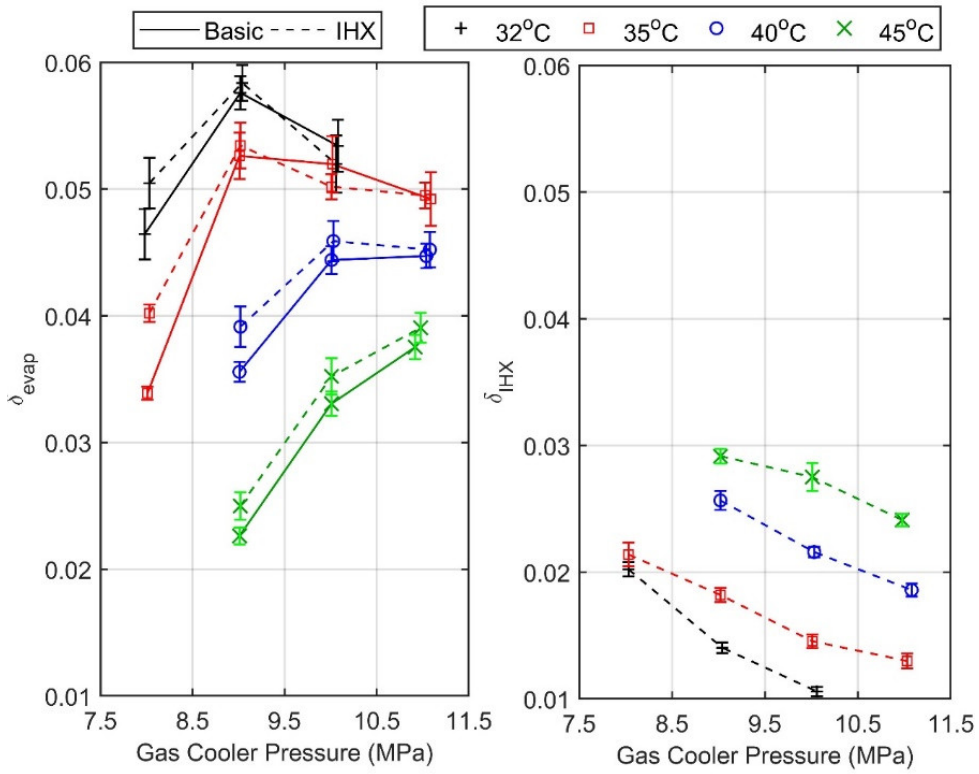

Fig. 4.32 Effect of operating parameters on the irreversibility contribution of evaporator and IHX

4.6 Summary

A prominent research gap of effect of gas cooler side air velocity on energetic and exergetic parameters are highlighted apart from the novelty of the study which is based on a CO_2 refrigeration setup. The experimental investigation is carried out covering the warm climate condition up to 45°C, where in the available literature is scarce. The summary outcome is following:

- The mass flow rate of refrigerant in IHX system is lower than that in basic cycle, which is due to the increased specific volume in IHX cycle. The maximum reduction of mass flow rate in IHX recorded is 11.2%. The effectiveness of IHX increase with decrease in compressor discharge pressure and evaporator pressure.

- The maximum rise in compressor discharge temperature for IHX cycle recorded is about 24ºC for 45ºC ambient temperature. While, gas cooler side air velocity has insignificant effect on the compressor performance.
- COP and exergetic efficiency for the IHX cycle is higher compared to basic cycle and the improvement increases with increase in ambient temperature or with decrease in evaporator temperature. The maximum improvement in COP and exergetic efficiency of IHX cycle recorded are 5.70% and 5.05% respectively.
- The approach temperature is found comparatively lower for IHX cycle, especially at extreme ambient condition and is found to decrease with increase in gas cooler side air velocity but, at the expense of increment in fan power, this potentially has negative affect on the overall cycle COP.
- Sensitivity analysis is carried out for various fan efficiency on the overall system COP for various air flow rate and operating conditions. For a fan with 75% efficiency, operated at air velocity of 1 $m \cdot s^{-1}$, a contribution of up to 0.152% on overall system efficiency is recorded for specific operating conditions in high ambient. Due to typical nature of fan power, a rather lower air speed near 1 $m \cdot s^{-1}$ is found to be optimum for most applications.
- The effect of air velocity over the system COP and exergetic efficiency are significant for both basic as well as IHX cycle.
- Irreversibility contribution of gas cooler followed by compressor and expansion valve are found significant at lower ambient temperature. While, at higher ambient, expansion valve followed by compressor and gas cooler contribute maximum towards system irreversibility. IHX have least contribution towards exergy loss of the cycle.

Design and development of CO_2 test rig should be critically reviewed based on material selection (type and grade considering both physical and thermal properties), high pressure and low-pressure safety mechanism, component isolation system, proper insulation of components and appropriate charging guidelines (Kim et al., 2004). In this study, the experimental test rig is provided with both low pressure and high pressure cut off as well as well isolation valves. While experimentation it was ensured that the refrigerant populated components (for example, receiver, liquid lines etc.) were properly insulated to avoid rapid saturation pressure fluctuations. Charging the system is critical and needs prior training. In the present work, proper training was provided to the research scholar by expert from the fabricator. The CO_2 system has high pressure at standstill, consequently, the system need to be de-charged after experimentation to avoid pressure gain in the components as the ambient temperature rises. Release of CO_2 in the atmosphere while de-charging should be also critically reviewed to avoid Asphyxiation based on the site location. The location of experimentation should be properly ventilated with free moving space. The electrical lines, switches and control panels should be properly designed and earthed for shock free experimentation. There should be a main control switch a little away from the test rig location to ensure power cut off in case of unexpected failure of the machine